CFSTI PRICES

H.C. $ 3.00 ; MN .65

Lawrence Radiation Laboratory

UNIVERSITY OF CALIFORNIA

LIVERMORE

UCRL-50284

AN APPROACH TO THE STUDY OF LIGHT ARMOR

Mark Wilkins

Charles Honodel

David Sawle

June 13, 1967

DISCLAIMER

AN APPROACH TO THE STUDY OF LIGHT ARMOR

ABSTRACT

This report outlines the first step in a program to obtain a fundamental understanding of the relationship that properties of materials have on the effectiveness of light armor. Two experimental diagnostic approaches have been used – high speed cameras and 600 kV flash x rays. Theoretical models of material behavior have been incorporated into a two-dimensional elastic-plastic computer program. Examples of projectile penetration are given for sharp- and blunt-nosed projectiles.

INTRODUCTION

The design of armor in the past has been primarily achieved with ballistic tests on a large variety of materials. Correlation of the ballistic behaviour and the mechanical properties of materials has lead to an empirical understanding of how armor functions. However, the correlations have not been entirely satisfactory in determining which material properties are important. Some of the reasons why ballistic tests have not yielded sufficient armor design information are:

- There is more than one mechanism operating at the same time in the defeat of penetration. The separate effects cannot be readily sorted out by the normal ballistic test approach to the problem.
- The dynamic properties of armor materials are not understood.
- The material properties of the projectile have an important effect on the target penetration; however, standard rounds of AP ammunition do not have the same material strengths. These facts upset any critical correlation made with various target materials.
- Composite armor introduces stress wave interactions from wave reflections at boundaries that further complicate the understanding of penetration mechanics.

These interactions, and the properties of material, constitute the major problem in armor design.

A 10 or even 5% weight reduction is a very important improvement when designing lightweight armor for helicopters. Also, for the lightweight armor now in use, it is not known what the effect will be if other than standard AP steel core bullets are employed. This points out the need to understand how armor defeats penetration and what the important physical parameters are.

This report describes progress on a program to achieve a fundamental understanding of the relationship that properties of materials have in defeating penetration by projectiles. The research is concentrated on projectile velocities characteristic of small firearms, i.e., ~2700 ft/sec and target materials characteristic of light armor, (defined as a material or composite of materials that defeat penetration at an areal density less than the areal density required by ballistic steel for the same ballistic threat).

PHILOSOPHY

The dominant role in the problem of light armor penetration mechanics is played by the inelastic behaviour (yield and plastic flow) of the interacting materials. The inelastic behaviour of a particular material is described by constitutive equations, which relate the stress tensor to the strain tensor. If the exact constitutive relations for the materials of interest were known, then a computer could be used to solve the equations of motion for any given practical problem.

Unfortunately this is not the case. The constitutive relations are not known and, in fact, one cannot even say with certainty which of the physical quantities characterizing the materials needs to be put into the constitutive equations in order to adequately describe armor penetration.

It is felt that one can develop adequate constitutive relations by choosing possible relations for which the computer solutions best agree with experiment. Thus, the important physical parameters characterizing armor materials could be isolated. It is not expected to describe material behaviour over a wide range of conditions, but rather to describe the outstanding features of the real phenomena for the ballistic problem at hand. In this work we will purposely stay close to idealizations. For example, perfect plasticity is an appropriate idealization for metals since it contains most of the essential features of the real phenomena, i.e., the model provides shear strength and accounts for the structure of stress waves.

A model of dynamic yielding was developed to learn how important dynamic effects might be in the context of ballistic experiments.

EXPERIMENTS

Penetration experiments can be divided into two types:

- The effects of a projectile on various targets.
- The effect of the target on the projectile.

It is well known that bullet-shaped projectiles are more effective for penetration than blunt projectiles. To defeat a bullet-shaped projectile an initial target requirement might be to destroy the bullet shape so as to make the projectile blunt. This is what occurs when AP bullets strike ceramic-faced armor. In order to study one effect at a time, projectiles of right circular cylinders and bullet-shaped cylinders were made with the nominal dimension of a 30-calibre round (cylinder length 0.9 in., diameter 0.3 in.). These projectiles were all fabricated from the same high strength steel (Fig. 1).

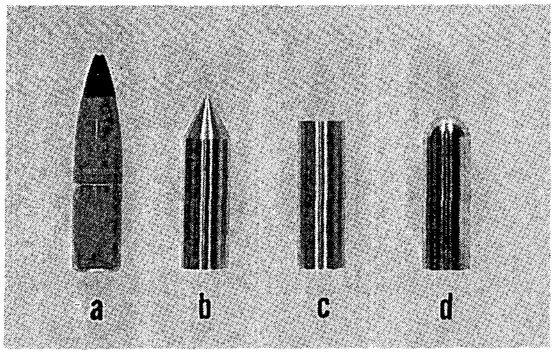

Fig. 1. Projectiles. a) 30-calibre AP bullet. b,c,d) Bullet simulators made from Allegheny steel 609, Rc 54-56, weight: 8.32 g.

A launching system was constructed to accelerate the cylinders to velocities ranging from 1000 to 3500 ft/sec (Fig. 2) Framing and streaking cameras recorded the response of the projectile and target during the collision. The experiments and calculations presented here were done to check out the methods for the research program. Aluminum was chosen as the target material because the physical properties are well known and there is not a significant strain-rate effect so that elastic-plastic theory applies.

Table I gives the parameters used in the experiments. The first series of experiments studied the effect of the projectile on the target. A Model 192 framing camera and a Model 100 streaking camera measured the motion of the rear surface of the targets (Fig. 3). The second series of experiments was primarily intended to study the effect that a hard target has on a projectile. Three channels of 600-kV x rays provide the means for observing the time sequence of events in the interior of a target.

The velocities of the projectiles were recorded by a laser velocity trap, which also provided the synchronization signal for the cameras and the x-ray units.

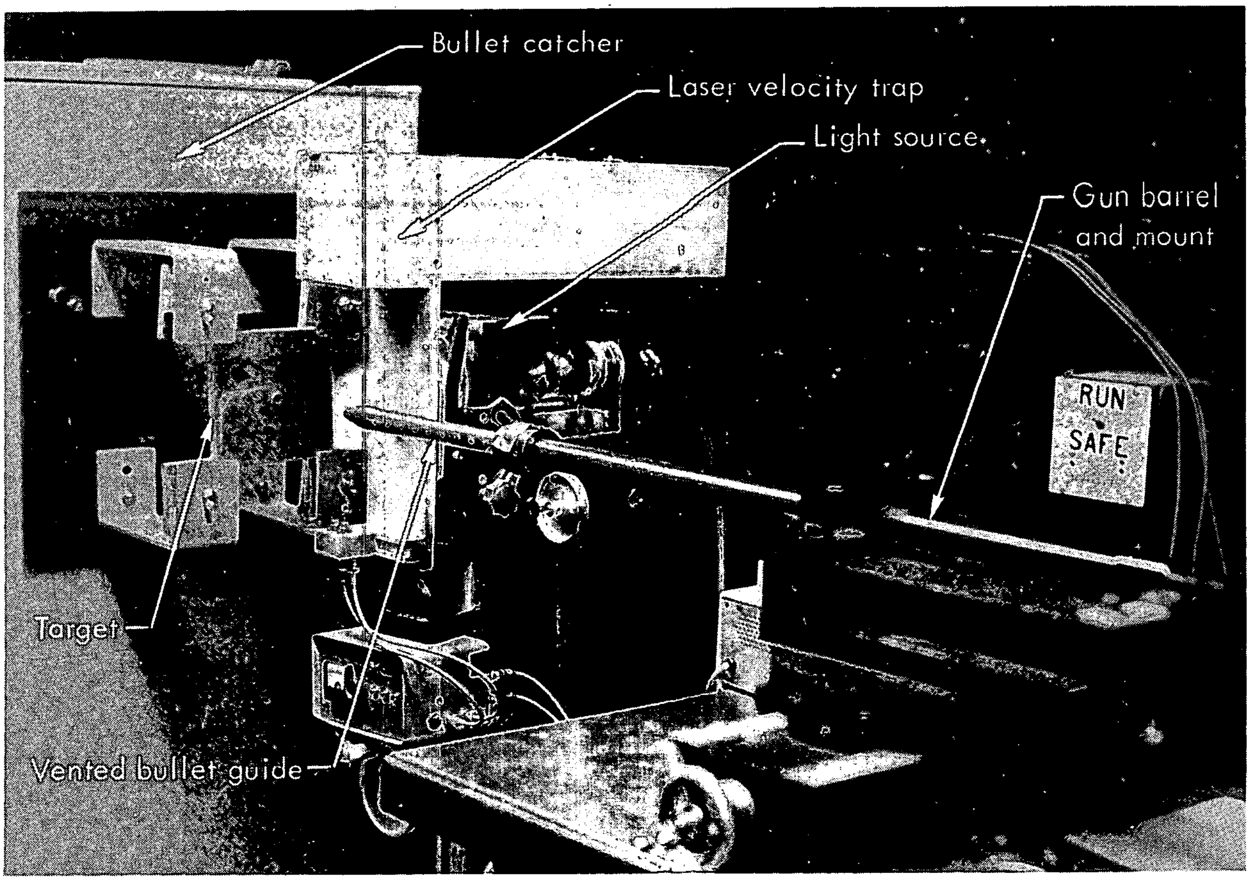

Fig. 2. Projectile launcher.

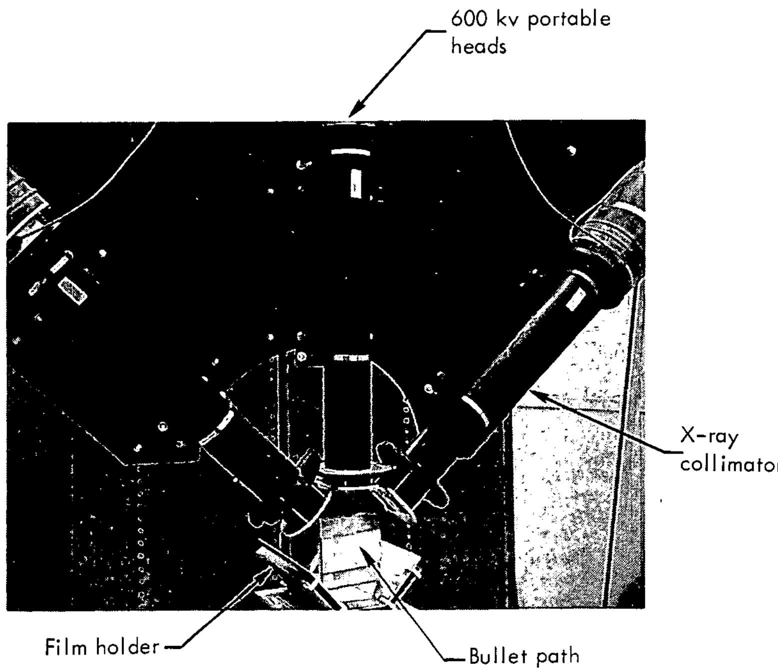

Fig. 3. Flash x-ray experimental set up.

Table I. Experiments.[a]

A. Effects on Target

Experiment	Target (6 in. × 6 in.)	Projectile: Shape (see Fig. 1)	Projectile: Velocity	Result
355-BE-4	3/4 in. thick Al	c	0.075 cm/μsec (2460 ft/sec)	Fig. 4 complete penetration
35-BE-5	1 in. thick Al	c	0.095 cm/μsec (3117 ft/sec)	Fig. 5 complete penetration
355-BE-6	1-1/2 in. thick Al	c	0.094 cm/μsec (3084 ft/sec)	Figs. 6 and 7 projectile stopped
355-BE-11	3/4 in. thick Al	c	0.091 cm/μsec (2986 ft/sec)	Figs. 8 and 10 complete penetration
355-BE-12	3/4 in. ($\frac{1}{4}+\frac{1}{4}+\frac{1}{4}$) laminated Al	c	0.090 cm/μsec (2953 ft/sec)	Fig. 9 complete penetration
355-BE-13	1 in. thick Al	b	0.084 cm/μsec (2756 ft/sec)	Fig. 11 complete penetration
355-BE-9	1-1/2 in. thick Al	b	0.088 cm/μsec (2890 ft/sec)	Figs. 12 and 13 complete penetration
362-AC-5	0.3 in. alumina + two laminates of 0.25 in. fiberglas	a	0.082 cm/μsec (2694 ft/sec)	Fig. 14 complete penetration
362-AC-7	0.5 in. thick Al	a	0.081 cm/μsec (2667 ft/sec)	Fig. 15 complete penetration

B. Effects on Projectile

Experiment	Target (2 in. × 6 in.)	Projectile: Shape	Projectile: Velocity	Result
353-BC-1	0.3 in. thick Alumina 0.5 in. thick Al	b	0.093 cm/μsec (3050 ft/sec)	Fig. 16 projectile stopped
353-BC-2	0.3 in. thick Alumina 0.125 in. thick Al	b	0.093 cm/μsec (3050 ft/sec)	Fig. 17 complete penetration

[a]All aluminum is 6061-T6.

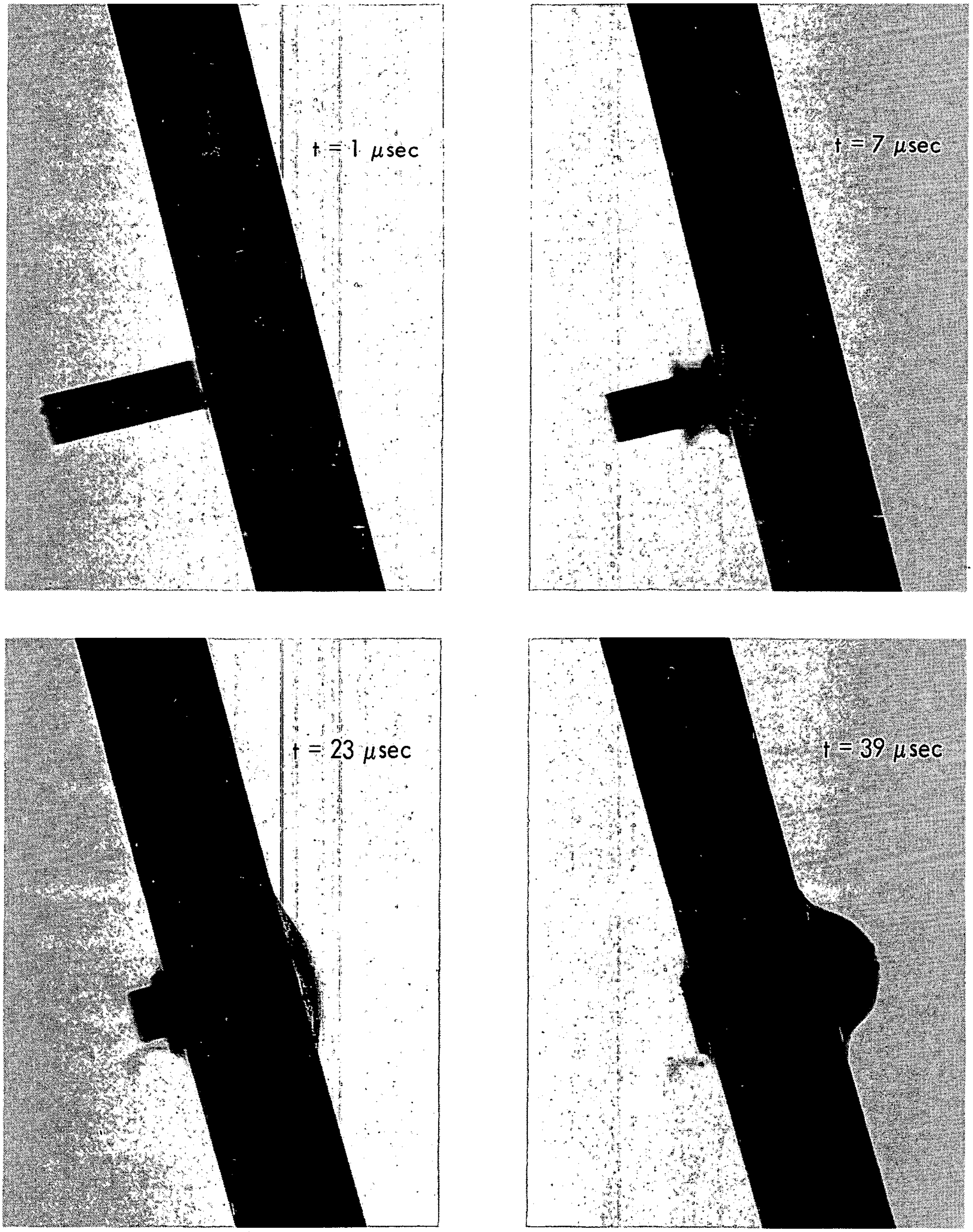

Fig. 4. Steel cylinder, velocity 2460 ft/sec, striking a 3/4 in. thick aluminum target. Time measured from impact. (Exp. 355-BE-4).

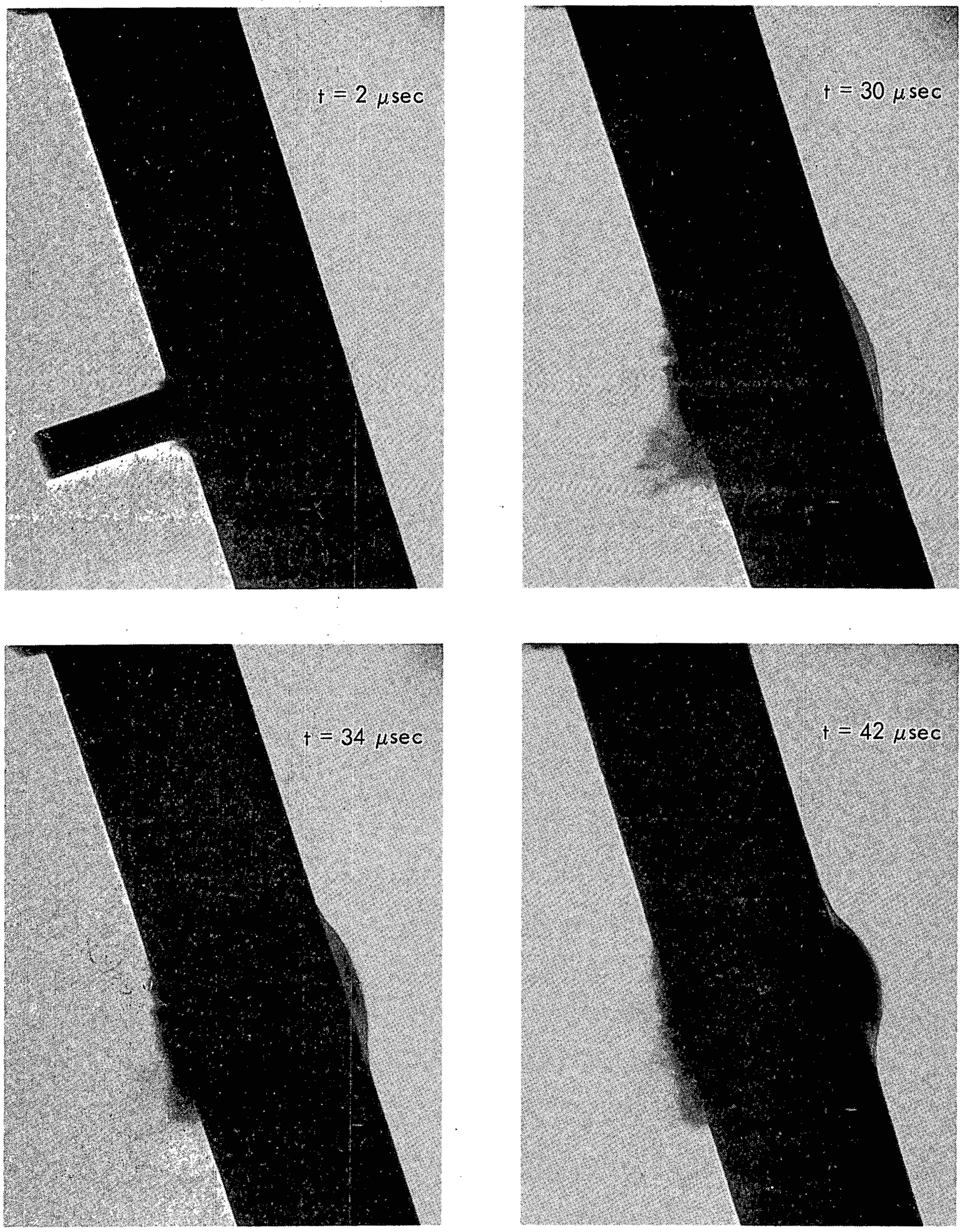

Fig. 5. Steel cylinder, velocity 3117 ft/sec, striking a 1 in. thick aluminum target. Time measured from impact. (Exp. 355-BE-5).

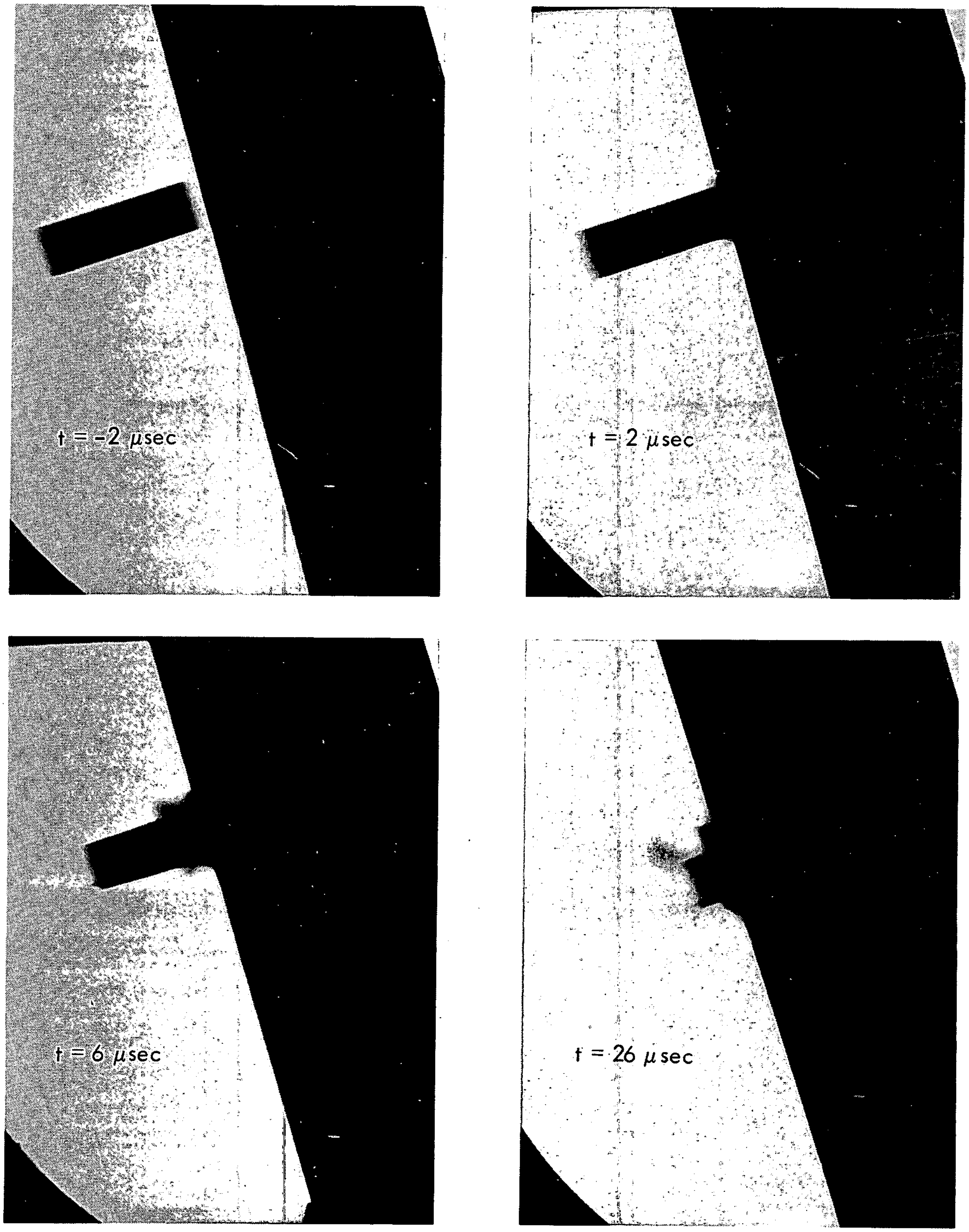

Fig. 6. Steel cylinder striking, velocity 3084 ft/sec, striking a 1-1/2 in. thick aluminum target, time in μsec from impact. (Exp. 355-BE-6).

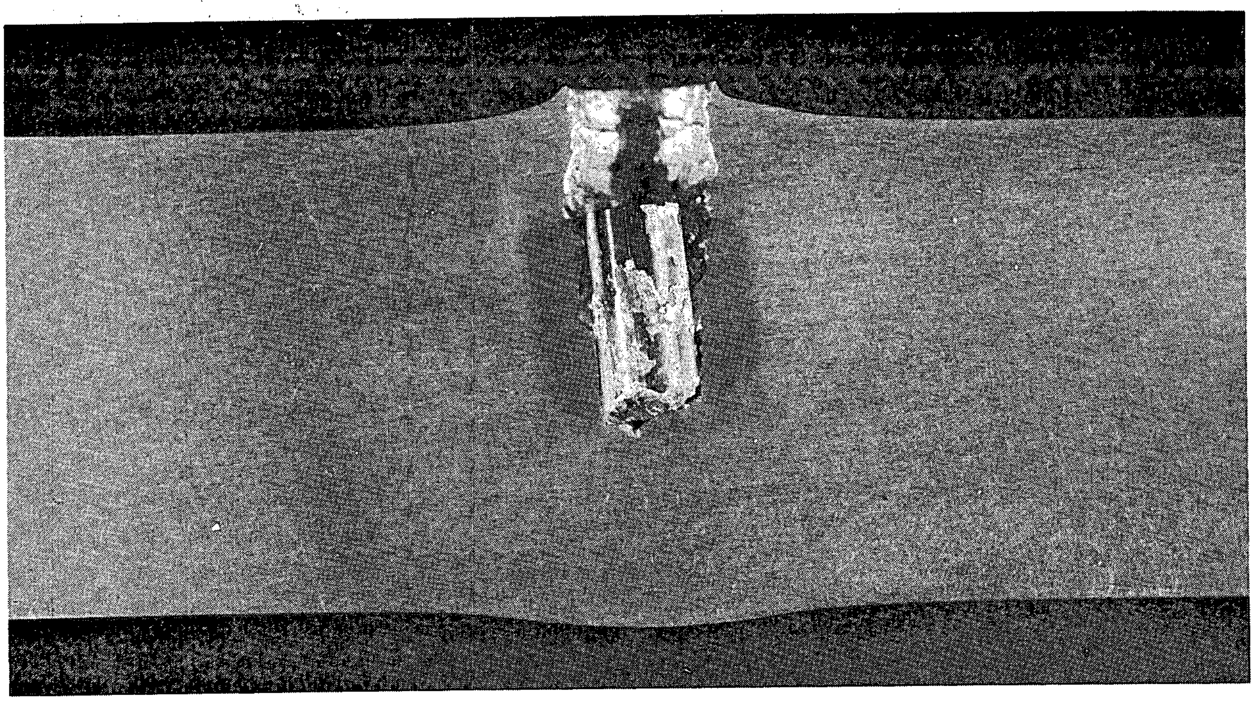

a. Projectile in place.

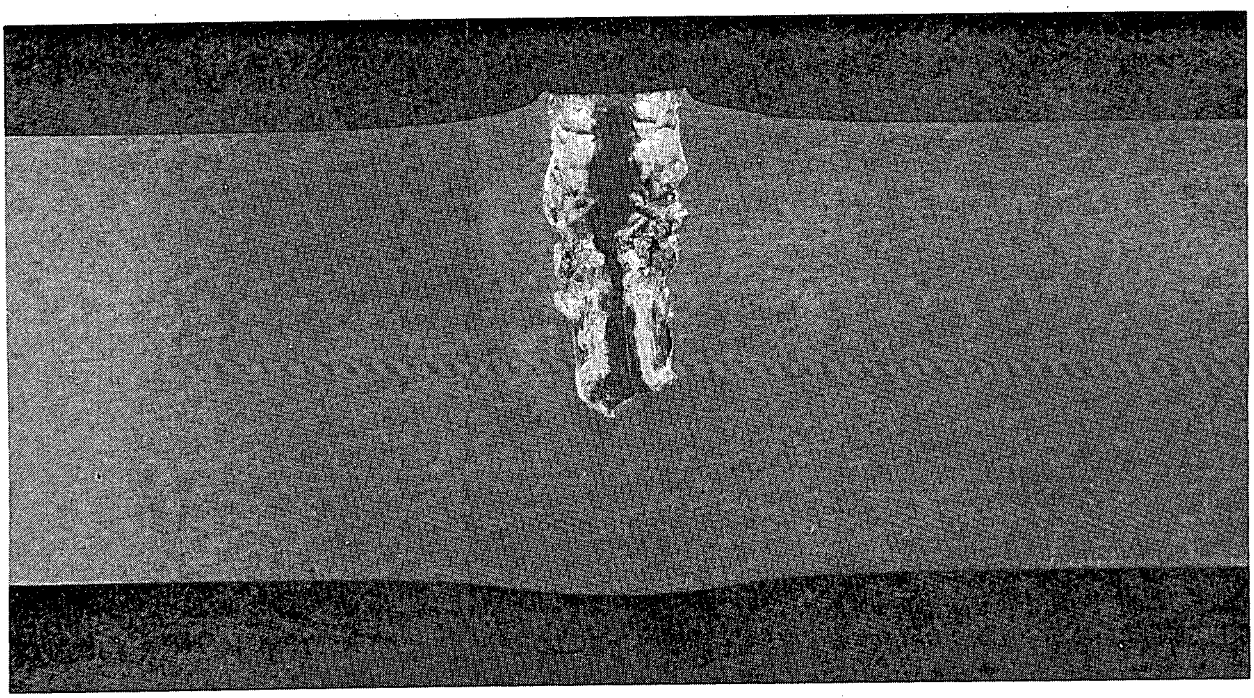

b. Projectile removed.

Fig. 7. Section views of 1-1/2 in. thick target of Fig. 6.

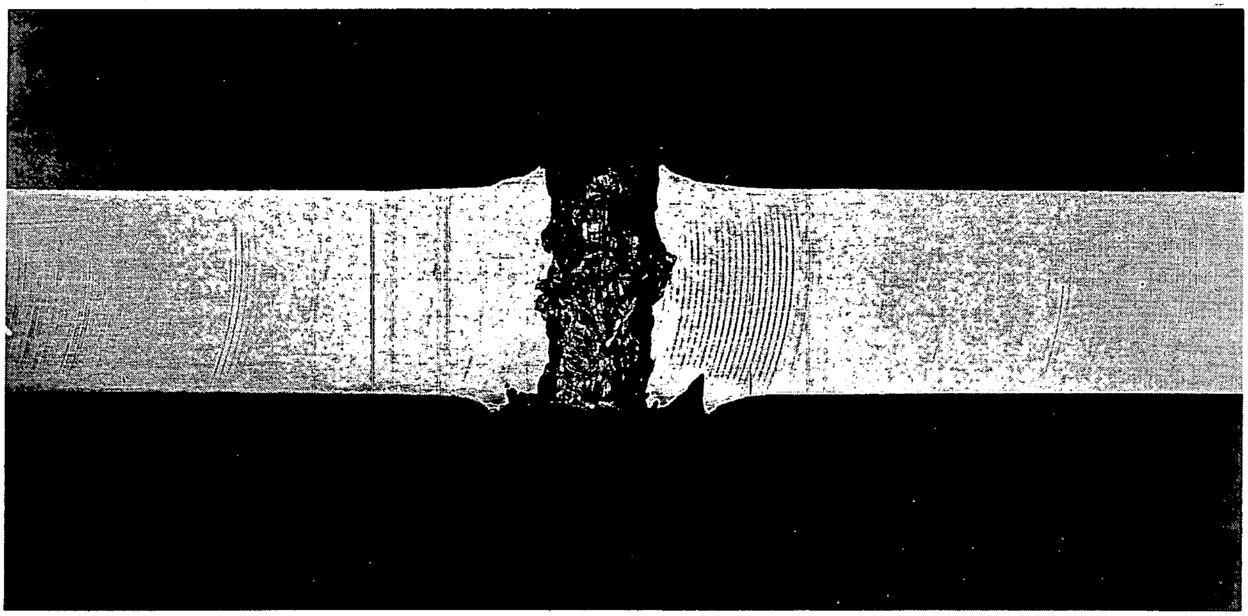

Fig. 8. 3/4 in. solid aluminum. Steel cylinder entered from top. Velocity 2986 ft/sec. (Exp. 355-BE-11).

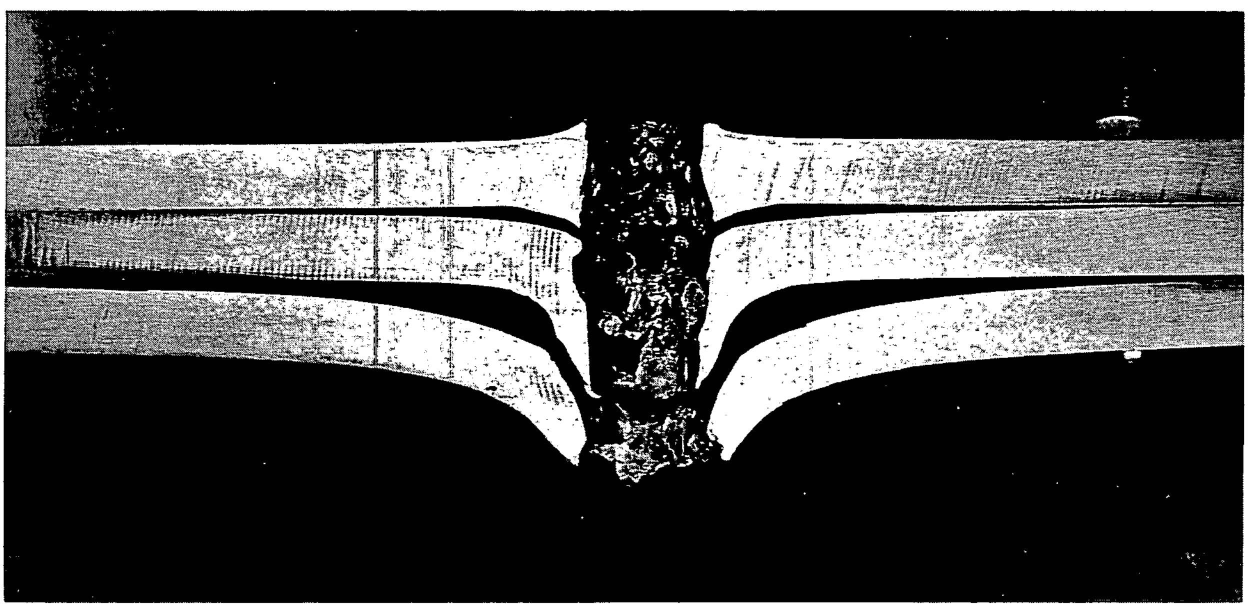

Fig. 9. Three laminates of 1/4 in. thick aluminum. Steel cylinder entered from top. Velocity 2953 ft/sec. (Exp. 355-BE-12).

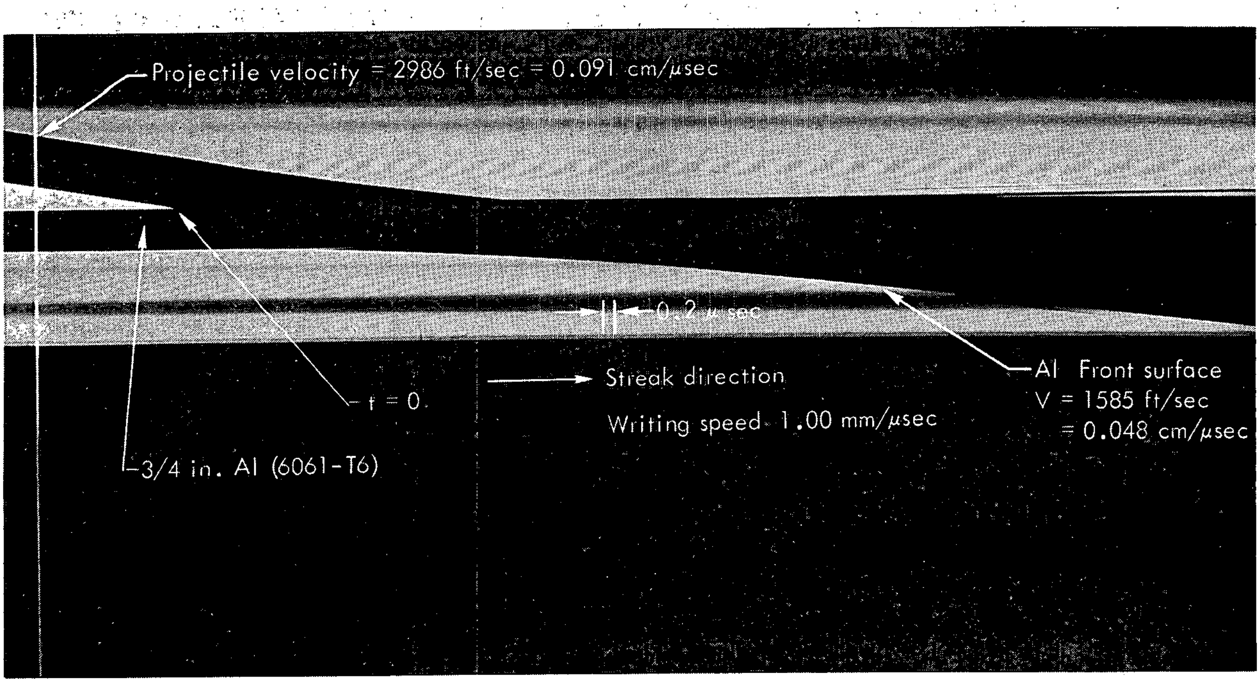

Fig. 10. Streak camera record showing the distance time history of the boundaries along the axis of a cylinder (type c) striking. 3/4 in. thick aluminum. (Exp. 355-BE-11).

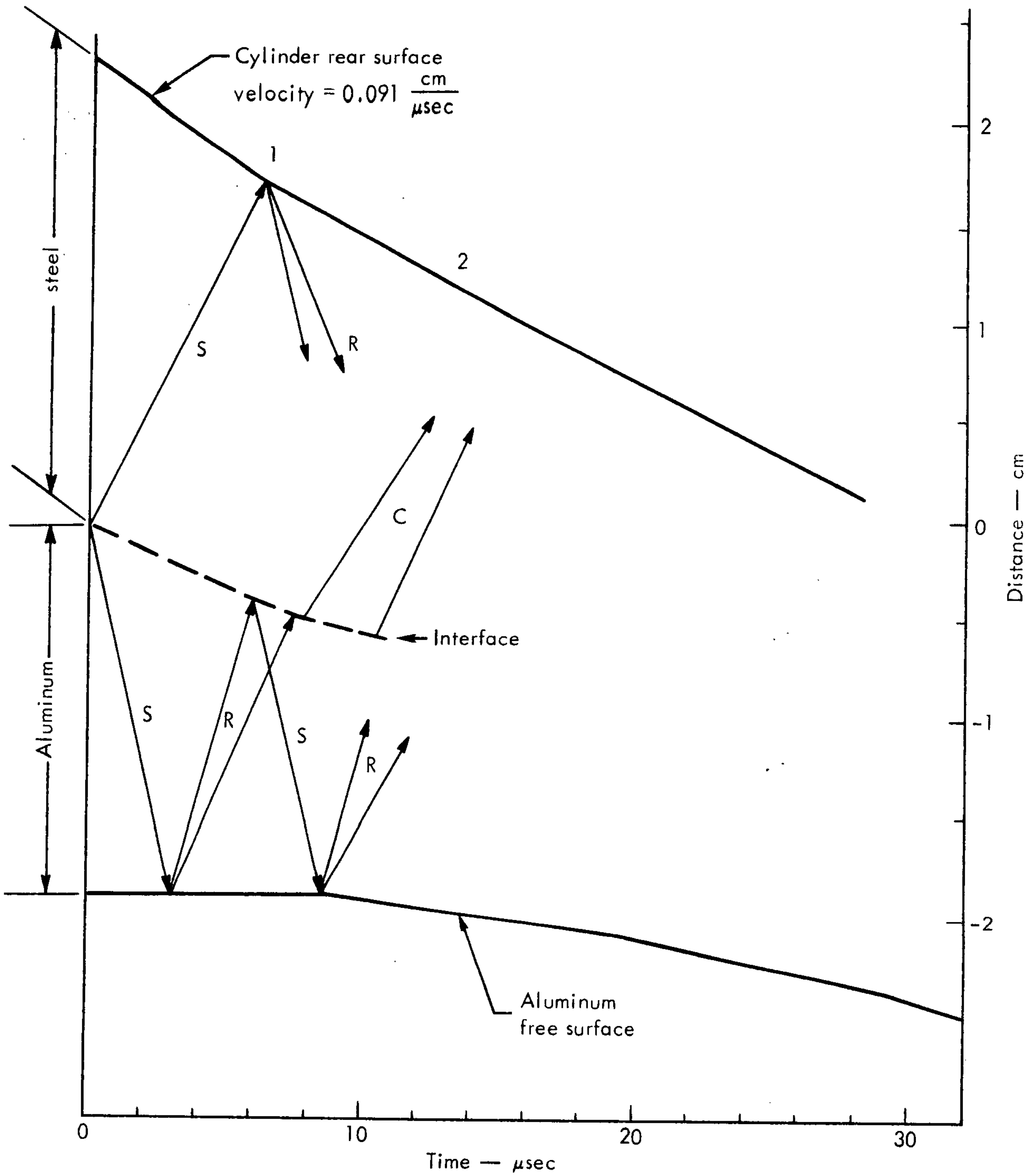

Fig. 10a. Analysis of streak record, Fig. 10; shocks, S; rarefactions, R; and interface position are calculated.

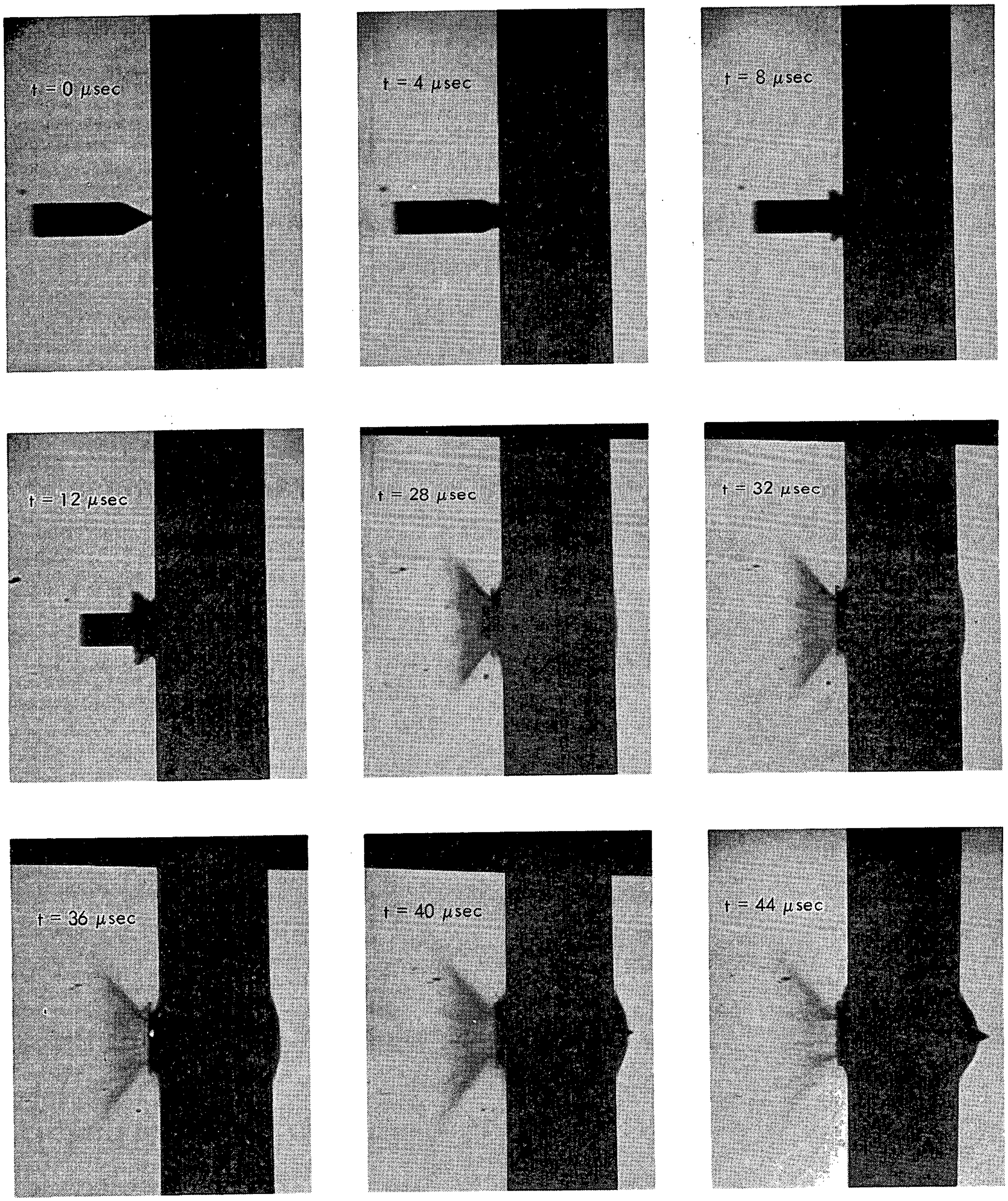

Fig. 11. Pointed cylinder (Type b, Fig. 1) striking a 1 in. thick aluminum target. Velocity 2756 ft/sec. (Exp. 355-BE-13).

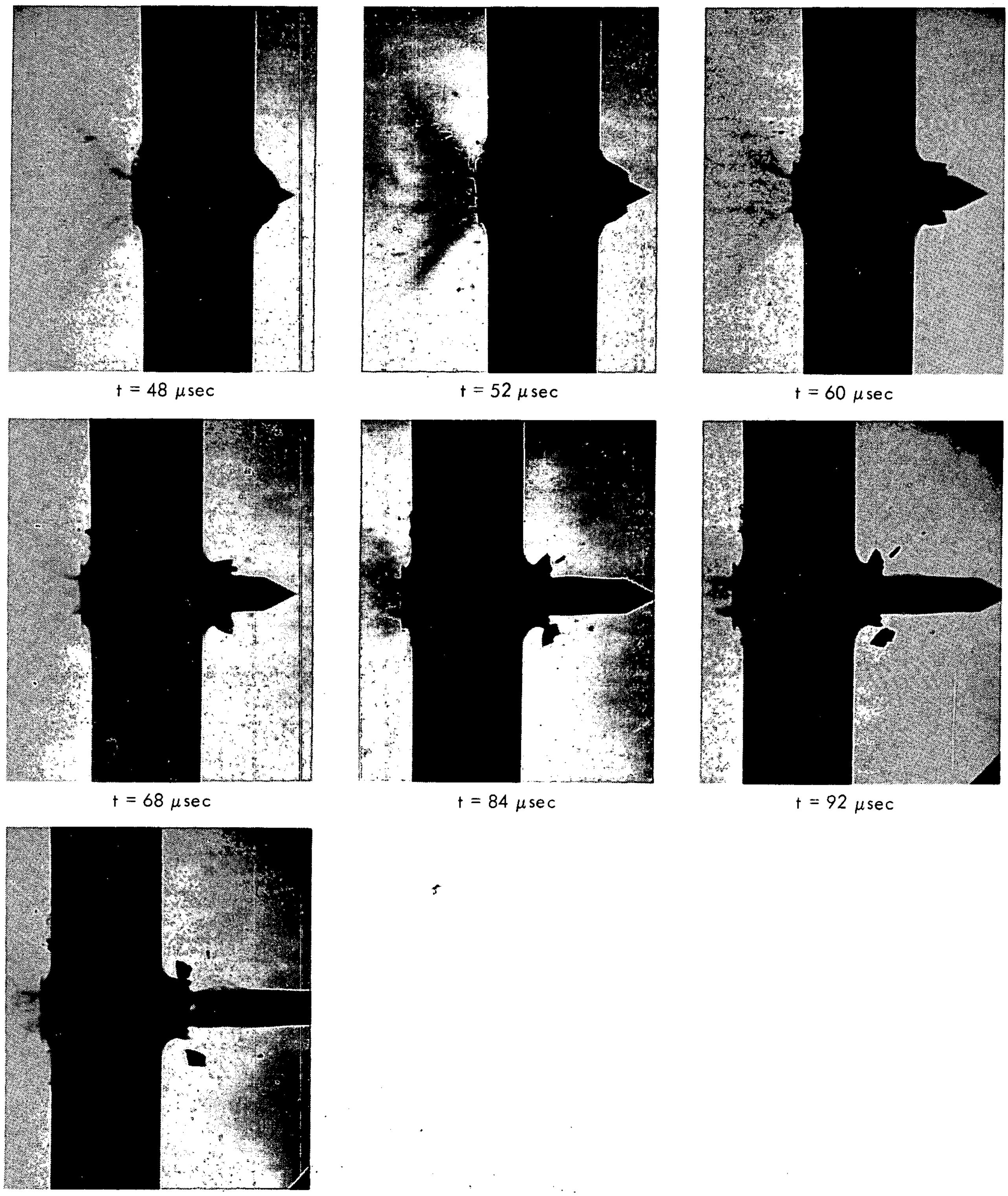

Fig. 11. Continued.

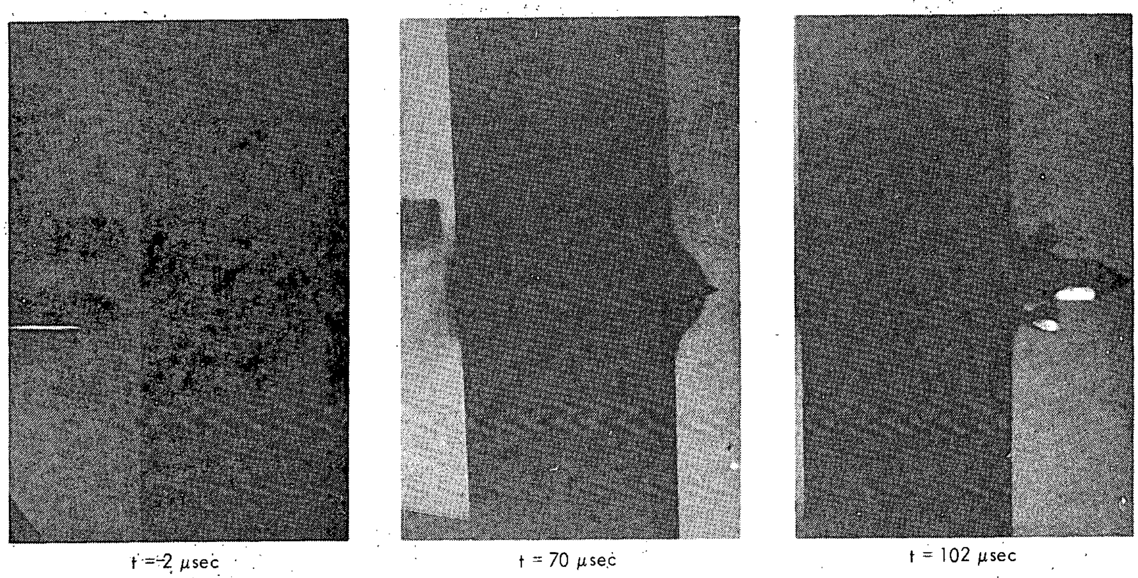

Fig. 12. Pointed cylinder (type b) penetrating a 1-1/2 in. thick aluminum target. Velocity 2890 ft/sec. (Exp. 355-BE-9).

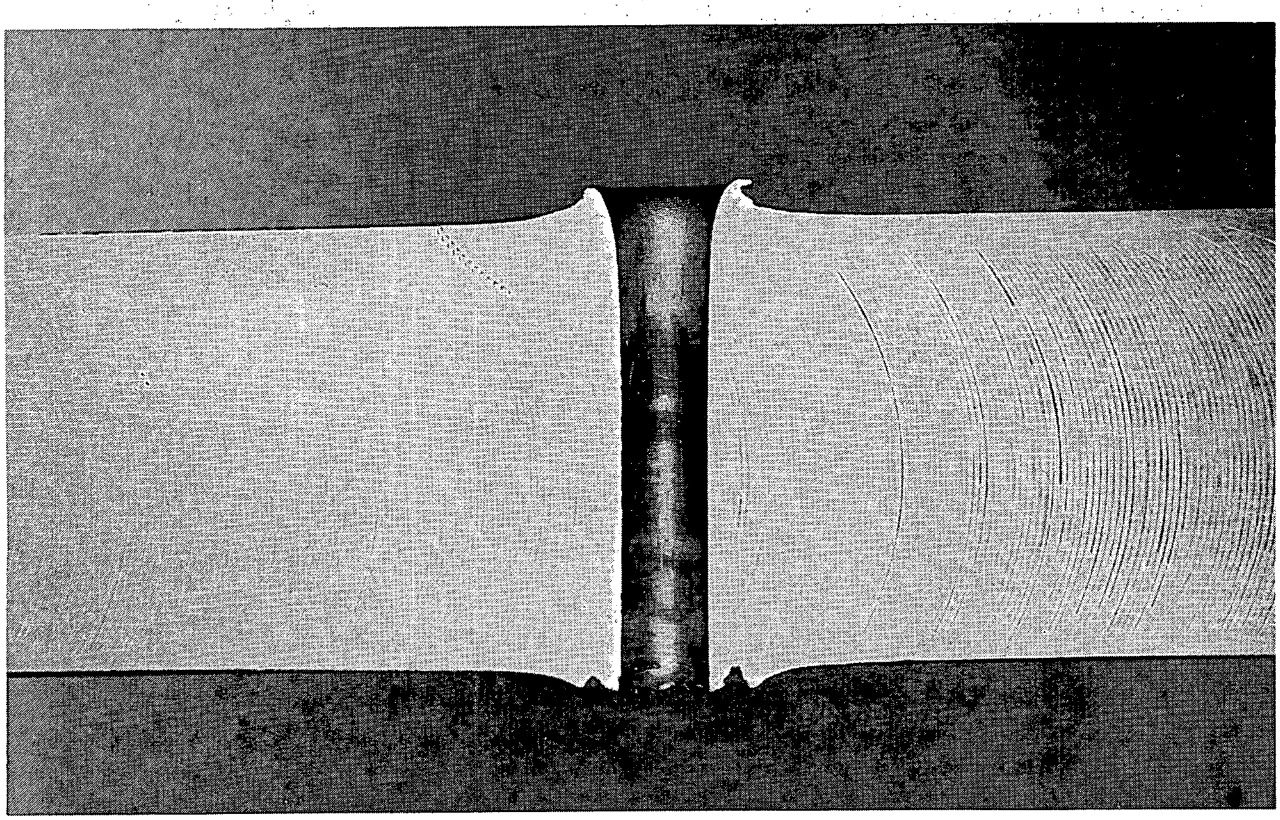

Fig. 13. Section view of 1-1/2 in. aluminum in Fig. 12, projectile entered from top.

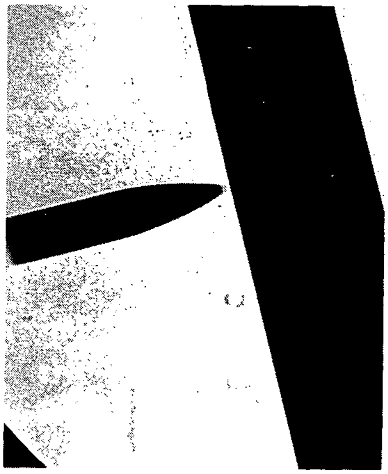

$t = 0\ \mu sec$

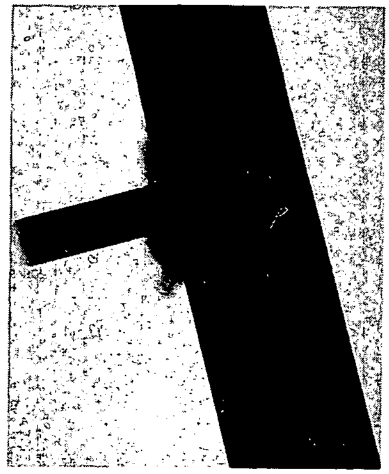

$t = 16\ \mu sec$

$t = 32\ \mu sec$

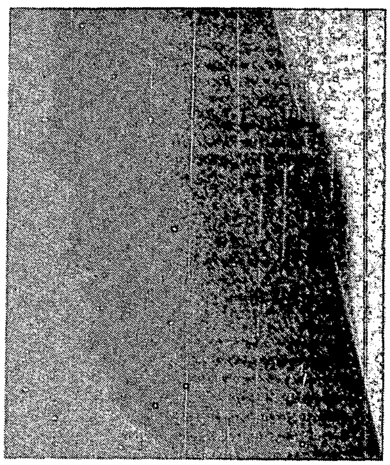

$t = 48\ \mu sec$

$t = 80\ \mu sec$

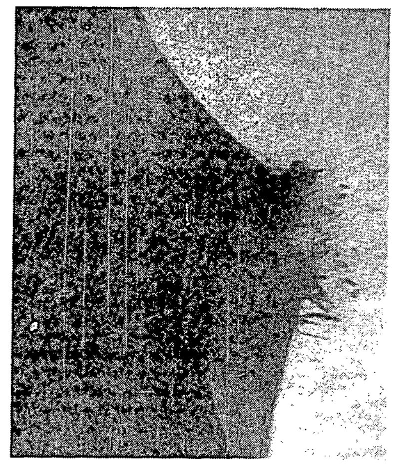

$t = 128\ \mu sec$

$t = 176\ \mu sec$

$t = 224\ \mu sec$

Fig. 14. AP bullet (type a, Fig. 1) striking a 0.3 in. facing of Al_2O_3 backed up by two laminates of 0.25 in. thick fibre glass. Velocity 2694 ft/sec. (Exp. 362-AC-5).

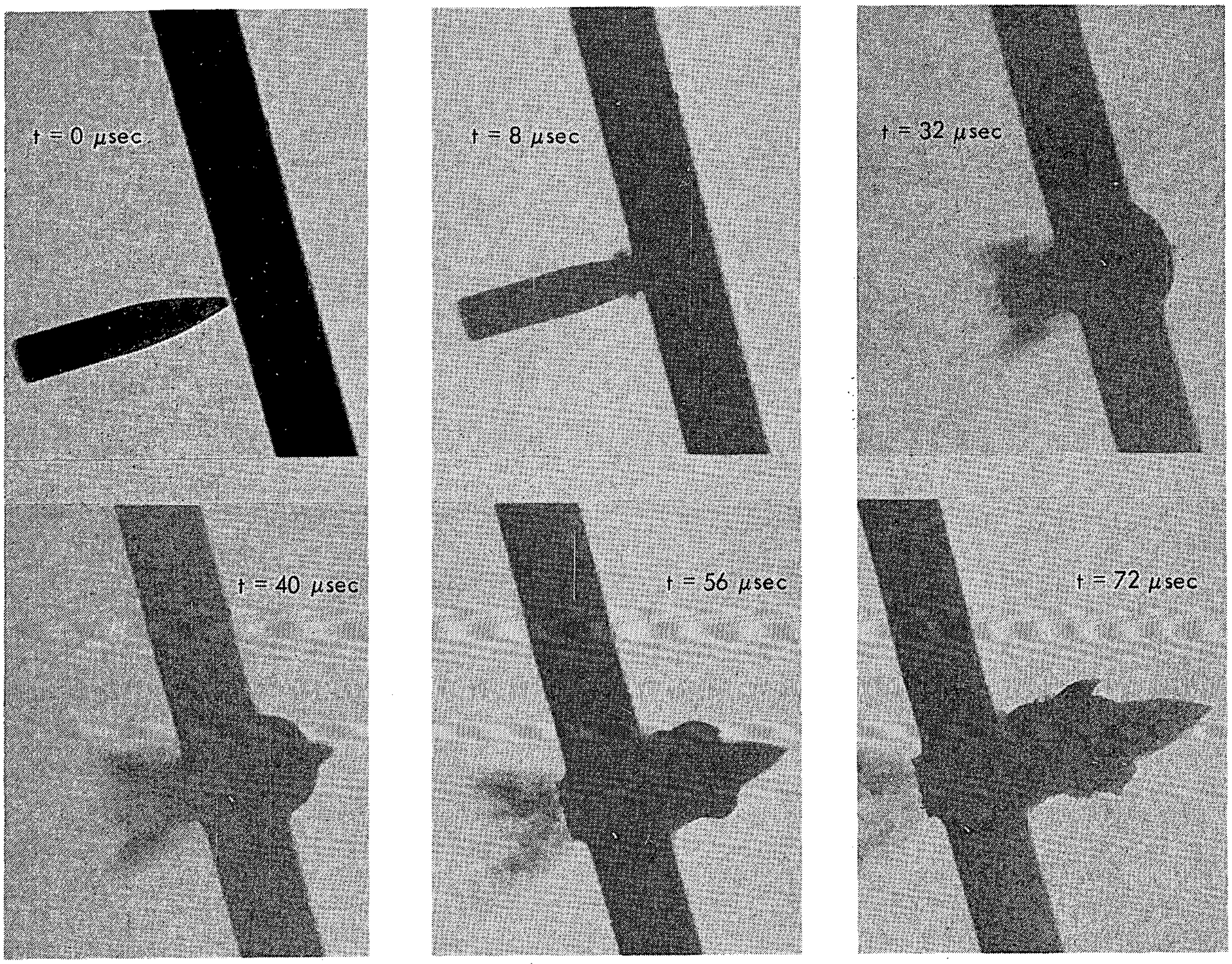

Fig. 15. AP bullet striking a 0.5 in. thick aluminum target. Velocity 2667 ft/sec. (Exp. 362-AC-7).

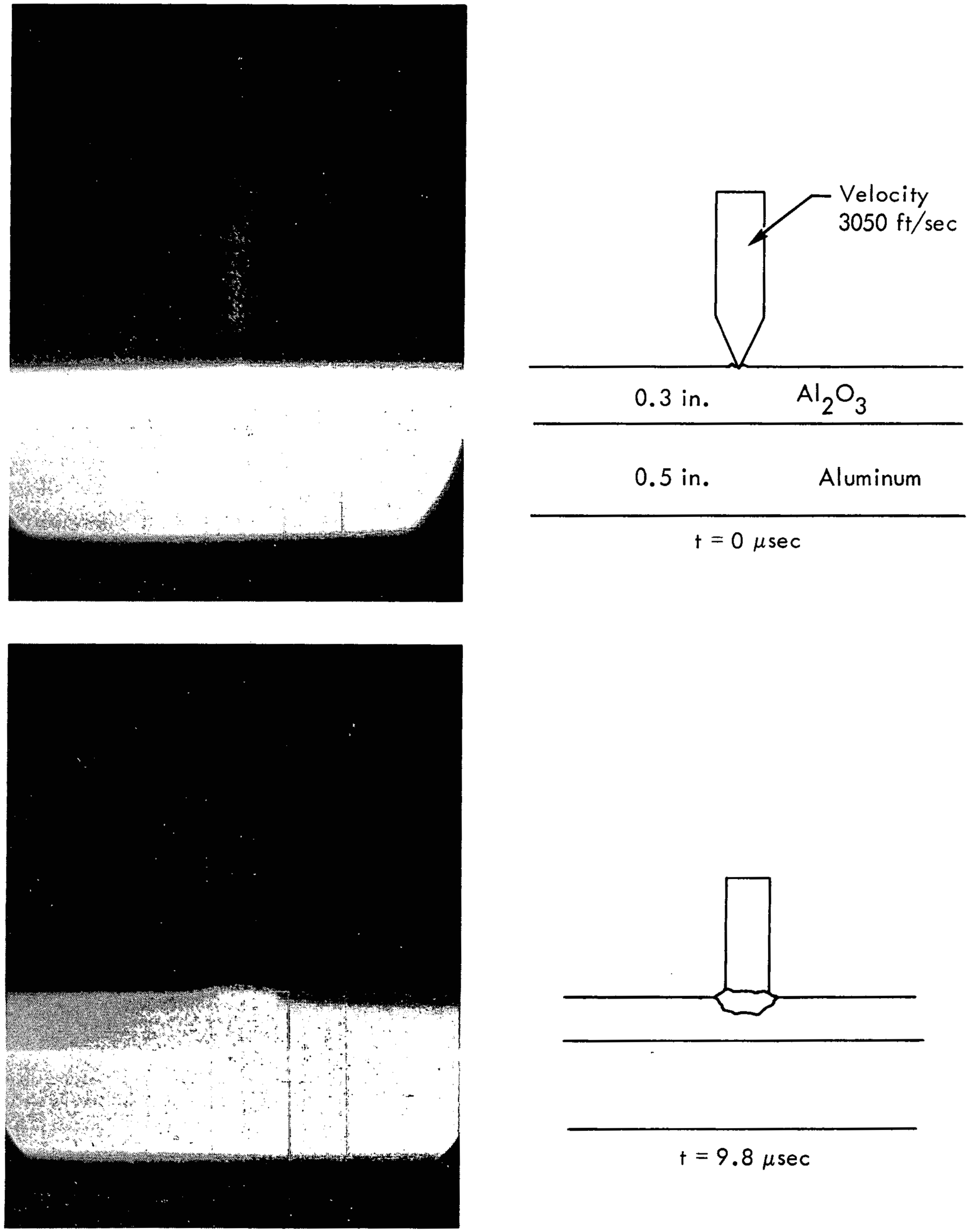

Fig. 16. Flash radiographs of a pointed cylinder (type b) striking a composite target 2 in. thick in the direction of the x rays. Exposure time: 0.02 μsec. (Exp. 353-BC-1).

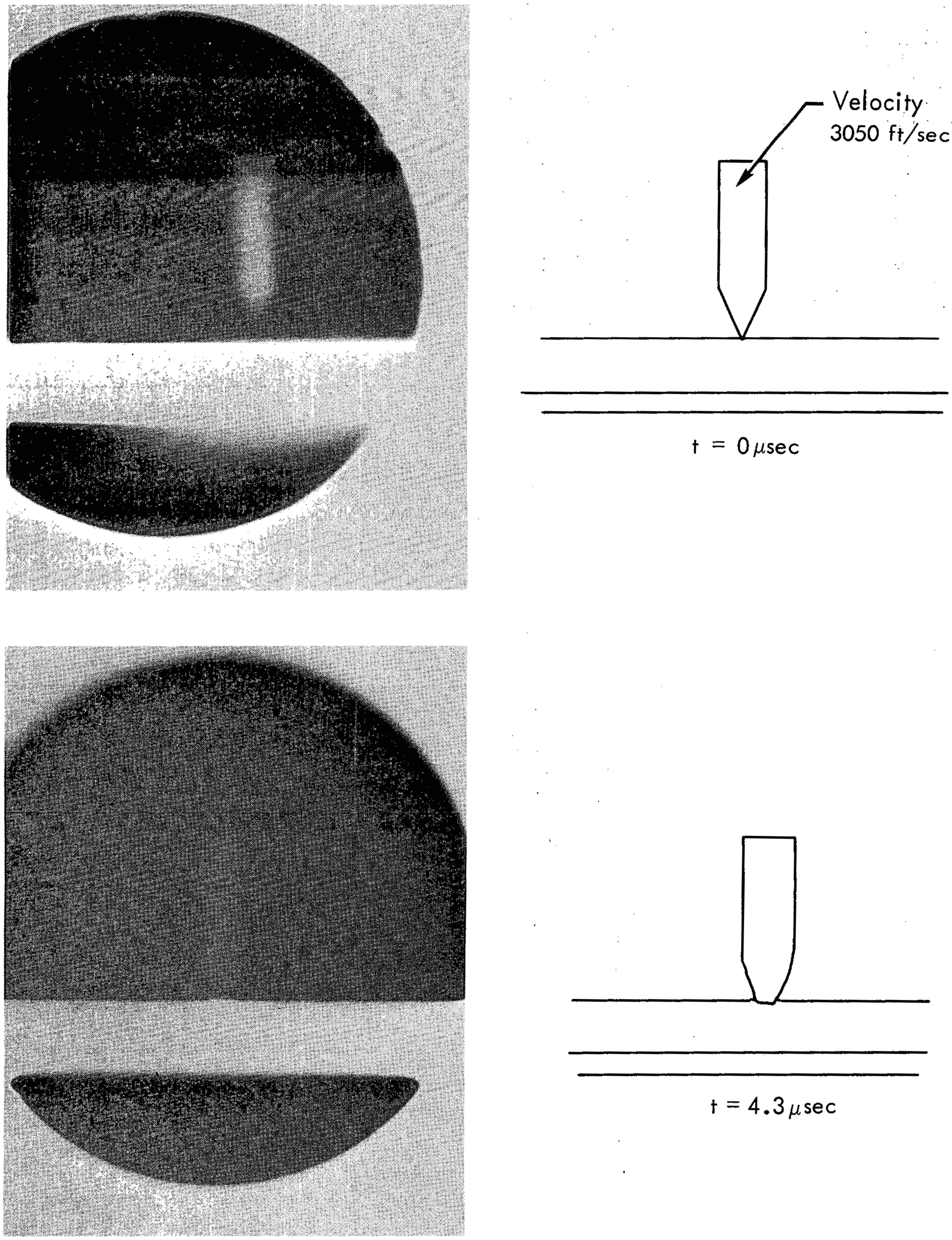

Fig. 17. Flash radiographs of a pointed cylinder striking (type b) a composite target 2 in. thick in the direction of the x rays. Exposure time: 0.02 μsec. (Exp. 353-BC-2).

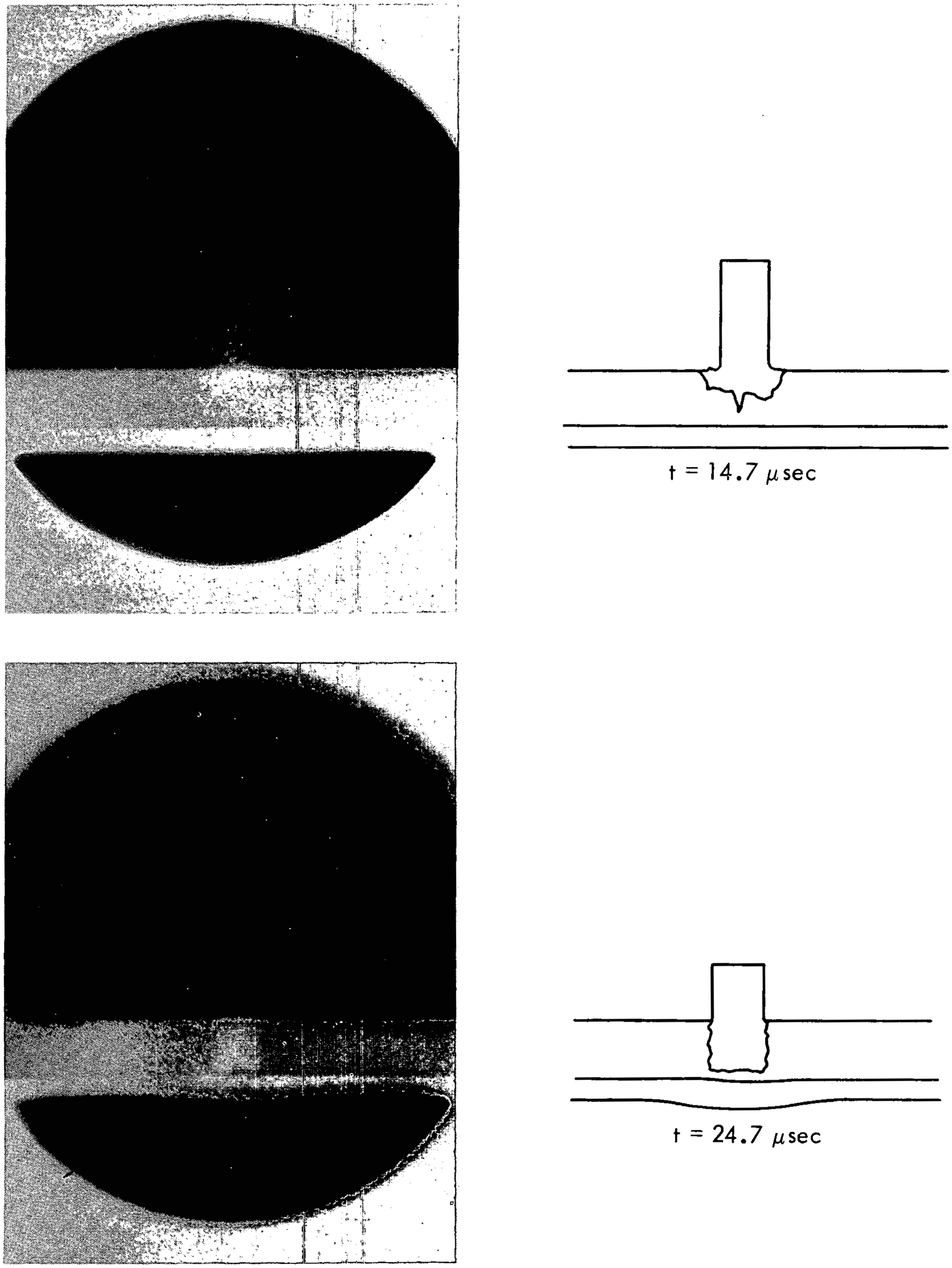

Fig. 17. Continued.

THEORY

The theoretical analysis is provided by the elastic-plastic computer program, HEMP, which solves the equations of continuum mechanics by finite difference methods.[1]

Basic Equations in the HEMP Code

(a) Equations of motion in x-y coordinates with cylindrical symmetry about the x-axis.

$$\frac{\partial \Sigma_{xx}}{\partial x} + \frac{\partial T_{xy}}{\partial y} + \frac{T_{xy}}{y} = \rho \ddot{x} ,$$

$$\frac{\partial T_{xy}}{\partial x} + \frac{\partial \Sigma_{yy}}{\partial y} + \frac{\Sigma_{yy} - \Sigma_{\theta\theta}}{y} = \rho \ddot{y} ,$$

$$\Sigma_{xx} = s_{xx} - (P + q) ,$$

$$\Sigma_{yy} = s_{yy} - (P + q) ,$$

$$\Sigma_{\theta\theta} = s_{\theta\theta} - (P + q) .$$

(b) Equation of continuity:

$$\frac{\dot{V}}{V} = \frac{\partial \dot{x}}{\partial x} + \frac{\partial \dot{y}}{\partial y} + \frac{\dot{y}}{y}$$

(c) Energy equation:

$$\dot{E} = - (P + q) \dot{V} + V (s_{xx}\dot{\epsilon}_{xx} + s_{yy}\dot{\epsilon}_{yy} + s_{\theta\theta}\dot{\epsilon}_{\theta\theta} + T_{xy}\dot{\epsilon}_{xy}) .$$

(d) Equation of state:

1. Stress components

$$\begin{cases} \dot{s}_{xx} = 2\mu\left(\dot{\epsilon}_{xx} - \frac{1}{3}\frac{\dot{V}}{V}\right) + \delta_{xx} , \\ \dot{s}_{yy} = 2\mu\left(\dot{\epsilon}_{yy} - \frac{1}{3}\frac{\dot{V}}{V}\right) + \delta_{yy} , \\ \dot{s}_{\theta\theta} = 2\mu\left(\dot{\epsilon}_{\theta\theta} - \frac{1}{3}\frac{\dot{V}}{V}\right) , \\ \dot{T}_{xy} = \mu(\dot{\epsilon}_{xy}) + \delta_{xy} , \end{cases}$$

where

μ = shear modulus

δ = correction for rotation

2. Velocity strains

$$\begin{cases} \dot{\epsilon}_{xx} = \dfrac{\partial \dot{x}}{\partial x} ; \quad \dot{\epsilon}_{\theta\theta} = \dfrac{\dot{y}}{y} \\[2ex] \dot{\epsilon}_{yy} = \dfrac{\partial \dot{y}}{\partial y} ; \quad \dot{\epsilon}_{xy} = \dfrac{\partial \dot{y}}{\partial x} + \dfrac{\partial \dot{x}}{\partial y} . \end{cases}$$

3. Hydrostatic pressure

$$\begin{cases} P = a(\eta - 1) + b(\eta - 1)^2 + c(\eta - 1)^3 + d\eta E , \\[1ex] \eta = 1/V = \rho/\rho^0 . \end{cases}$$

4. Von Mises yield condition $\left(s_1^2 + s_2^2 + s_3^2\right) - (2/3)(Y^0)^2 \leq 0$

where

Y^0 = material strength,

(s_1, s_2, s_3) are the principal stress deviators.

These constitutive equations are appropriate for ductile metals and are the starting point for more sophisticated relations.

(e) Notation:

x,y	space coordinates
$\dot{x}$	velocity in x direction
$\dot{y}$	velocity in y direction
$\Sigma_{xx}, \Sigma_{yy}, \Sigma_{\theta\theta}$	total stresses
T_{xy}	shear stress
$s_{xx}, s_{yy}, s_{\theta\theta}$	stress deviators
$\epsilon_{xx}, \epsilon_{yy}, \epsilon_{\theta\theta}, \epsilon_{xy}$	strains
P	hydrostatic pressure
V	relative volume
E	internal energy per original volume
ρ	density
q	artificial viscosity: (quadratic "q")

The dot over a parameter signifies a time derivative along the particle path.

Elastic-Plastic Assumption

The material properties are described by the equation of state (d) above. The strength of materials appears as the parameter Y^0 in the yield condition (d.4). The equation of state as written corresponds to an elastic-perfectly plastic material. The physical assumption in this formulation will be examined in this section to establish a point of departure for the dynamic yield described in the next section.

It is convenient to write the yield conditions (d.4) in a more general form

$$\text{Yield Condition:} \quad f(s_1, s_2, s_3) = 0 \ . \tag{1}$$

In plasticity theory it is usually assumed that plastic behaviour is independent of the pressure. Therefore the condition for plastic flow is written in terms of the stress deviators, s_1, s_2, and s_3.

This expression states that in the principal stress space there is a boundary condition on the magnitude of the stresses. After this value has been attained, plastic flow begins. On a loading path prior to reaching the boundary condition $f(s_1, s_2, s_3) < 0$, and the material is in the elastic region.

By perfectly plastic flow it is meant that the function, $f(s_1, s_2, s_3) = 0$, retains its form during the whole process of plastic flow, i.e., $\dot{f} = 0$. This means there is no *strain hardening and that the material flows plastically under a constant yield stress.*

A considerable simplification is obtained by assuming that Eq. (1) is independent of a change in stress sign (absence of Bauchinger effect). The material thus behaves similarly in tension and compression.

By itself the yield condition is not sufficient to characterize the mechanical behaviour of a perfectly plastic material. It must be supplemented by a stress-strain relation for the plastic region. Plasticity theories assume that during plastic flow the rate of plastic strain is at any instant proportional to the instantaneous stress deviator. Stated mathematically:

$$\text{Plastic Flow Law:} \quad \begin{aligned} {}^{P}\dot{\epsilon}_1 &= \dot{\lambda} s_1 \\ {}^{P}\dot{\epsilon}_2 &= \dot{\lambda} s_2 \\ {}^{P}\dot{\epsilon}_3 &= \dot{\lambda} s_3 \end{aligned} \tag{2}$$

Here s_1, s_2, and s_3 are the principal stress deviators, ${}^{P}\dot{\epsilon}_1$, ${}^{P}\dot{\epsilon}_2$, ${}^{P}\dot{\epsilon}_3$ are the corresponding components of the plastic strain rate deviators and $\dot{\lambda}$ is a scalar plastic flow rate parameter. This parameter is different for different positions and different for the same position at different times. It is to be noted that the stresses s_1, s_2, and s_3 are not rate dependent by Eq. (2) but are proportional to a rate-dependent parameter through a rate-dependent constant. This is in contrast to elasticity theory which states that the stress is proportional to the strain so that stress and strain determine each other. Here the stress is proportional to the plastic strain rate so a state of plastic strain does not correspond to a unique state of stress.

Most theories of plasticity follow the experimental observation that there is no permanent change in volume due to plastic strain (plastic incompressibility). This can be stated mathematically as:

$$\text{Plastic Incompressibility:} \quad {}^P\epsilon_1 + {}^P\epsilon_2 + {}^P\epsilon_3 = 0 \tag{3}$$

The total strain, e, is considered to be the sum of the plastic strain, ${}^P\epsilon$, and the elastic strain, ${}^E\epsilon$.

$$e_1 = {}^P\epsilon_1 + {}^E\epsilon_1$$

$$e_2 = {}^P\epsilon_2 + {}^E\epsilon_2 \; ,$$

$$e_3 = {}^P\epsilon_3 + {}^E\epsilon_3 \; .$$

By the definition, Eq. (3), it is seen that the plastic strain is already a deviator. The elastic portion of the strain is recoverable, but the plastic portion is assumed to be permanent.

Equations (1), (2), and (3) express the fundamental assumptions of plasticity theory and are incorporated in the computer program where the von Mises theory is used for the yield condition.

The strength character of a material is revealed by dynamic tests where the elastic portion of the stress wave separates from the slower moving plastic portion. The stress wave thus shows a two-wave structure. Measurements on the elastic precursor can be interpreted in terms of the shear strength of the material. At higher stress levels the plastic portion of the wave moves faster than the elastic portion and only a single wave results. However, the strength character of material has a large effect on the shape of the stress wave behind the front.

Experiments that record the shape of stress waves can be used to infer the material strength at high pressures. Work is in progress to measure by means of manganin wire pressure transducers the profiles of waves propagating in materials of interest for armor.

Dynamic Yielding

In recent years the use of dislocation theory to predict elastic-plastic behaviour of materials has been very successful. Johnston and Gilman[2] and Gilman[3] have made major contributions in the field and have had excellent results using dislocation dynamics in the calculation of the mechanical properties of materials. J. Taylor[4] and

J. Johnson[5] have applied dislocation theory to describe the relaxation of an elastic precursor preceding a shock wave in one-dimensional strain geometry.

To gain insight into the importance of dynamic properties of materials in the armor problem, it seemed appropriate to include these effects in the calculational program. Presented here is a model of dynamic yielding based on dislocation theory.

The dynamic yield model is formulated so that a continuous time description of the material is provided. Thus, the states of the material at the shock front and behind the shock front can be described by dislocation dynamics. The past history of the material is recorded by the total plastic strain and the dislocation density.

Plastic Strain Rate

In terms of the motion of dislocations the plastic strain rate $\dot{\gamma}$ is given by:

$$\dot{\gamma} = bNW \tag{4}$$

where b is the Burgers vector, N the mobile dislocations density, W the average velocity of the dislocations.

Experiments show that the velocity of dislocations[3] is very well described by:

$$W = W_0 \, e^{-D/\tau_{eff}} \tag{5}$$

where D is a characteristic drag stress, W_0 the maximum dislocation velocity. τ_{eff} is the effective shear component of the applied stress, where $\tau_{eff} \geq 0$.

Increase in Dislocation Density

As a dislocation moves, it interacts with existing defect structures to form sources of new dislocations. Thus the rate of production of new dislocations is proportional to the distance they travel and to the total number.

$$\begin{aligned} dN &= \alpha NW dt, \\ dN/dt &= \alpha NW. \end{aligned} \tag{6}$$

In the shock transformations that are of interest here it may be assumed that it is the mobile dislocation density that increases. However, the density does not increase without bound. Interactions between dislocations such as the tangling between dislocations moving in two different slip planes or the annihilation process between dislocations of opposite signs lead to a fraction of the total mobile dislocations being lost to the plastic flow process. Taking this into account:

$$dN/dt = \alpha NW\ (1 - fN)\ , \tag{7}$$

substituting $NW = \dot{\gamma}/b = (d\gamma/dt)(1/b)$ from Eq. 1 gives

$$dN = \frac{\alpha}{b}\ (1 - fN)\ d\gamma . \tag{8}$$

The integration of the above equation, subject to the initial condition, $N = N_0$ for $\gamma = 0$, gives:

$$N = 1/f\ [1 + (fN_0 - 1)\ e^{-\alpha f\gamma/b}]\ . \tag{9}$$

Thus as γ increases, the number of mobile dislocations approaches a limit $N_{limit} = 1/f$.

Work Hardening

Plastic deformation is essentially the result of dislocations moving on slip planes. However, as more and more dislocations are produced to carry the plastic flow, there is a corresponding increase in the total number of interactions between dislocations. In addition to limiting the dislocation multiplication, the interaction processes have the net effect of placing a drag force on the mobile dislocations. The drag force exerted by the interactions requires an increase in the applied shear stress to maintain a given dislocation velocity. This phenomenon is called work hardening. A parameter that characterizes what has happened to a material subjected to applied stresses is γ, the plastic shear strain. Work hardening can therefore be described by an increase in the material strength as a function of γ. It might be considered that the amount of plastic distortion work would be a better parameter choice. Isotropy has been assumed here and there is no loading path dependence. It doesn't make any difference then which parameter is used to give the strength state of the material. They essentially serve the same role. What does make a difference is that the yield strength can be increased by the past history of the material. It will be convenient to describe the shear stress due to work hardening for use in the next paragraph by:

$$\tau_{WH} = [\gamma/(a + \gamma)]\ \tau_M \tag{10}$$

where a and τ_M are constants.

Effective Stress

The effective stress operating to drive the dislocations in the dislocation velocity equation, Eq. (5), represents the stress that is in excess of any background resistive stress, τ_R, present and the work hardening stress τ_{WH}. Therefore the effective shear stress, τ_{eff}, is written as:

$$\tau_{eff} = \tau_0 - (\tau_R + \tau_{WH}) \tag{11}$$

where τ_0 is the applied shear stress.

This formulation of the behaviour of materials allows pre-yield dislocation motion. A good measure of the applied shear stress is the octahedral shear stress.

$$\tau_0 = 1/\sqrt{3} \quad \sqrt{s_1^2 + s_2^2 + s_3^2} \tag{12}$$

where s_1, s_2, and s_3 are the principal stress deviators and are calculated following Hooke's Law.

Calculation of Yielding

A von Mises type yield condition imposes a limit Y^0 on the magnitude that the octahedral shear stress τ_0 may attain.

$$\tau_0 - Y^0 \leq 0 \ . \tag{13}$$

In the principal stress space the inequality (13), taken with the equal sign, describes a circle on a plane through the origin. The normal to the plane at the origin is equally inclined to the coordinate axes. (see p. 215 Ref. 1). The parameter Y^0 represents the material strength and determines the radius of the yield circle. When the stress deviators combine to give a value of τ_0 inside the yield circle the material is in an elastic state. If the stress deviators combine to fall outside the yield circle, plastic flow is assumed to occur. The inequality (13) in this case is satisfied by scaling the individual components of the stress tensor by Y^0/τ_0. By adjusting the components of the stress tensor in this manner the plastic flow law is satisfied, i.e. the plastic strain-rate vector remains normal to the yield surface. The assumption of plastic incompressibility is implicit in this formulation.

The maximum state of shear stress that the material may attain is considered to be the actual applied shear stress minus the component of stress corresponding to plastic flow.

$$\tau_y = \tau_0 - \mu \dot{\gamma} \Delta t , \tag{14}$$

where μ is the shear modulus and $\dot{\gamma}$ is the plastic strain as described above from dislocation theory.

A lower limit of the strength is imposed by:

$$\tau_y \geq (\tau_R + \tau_{WH}) . \tag{14a}$$

Now, the maximum shear strength τ_y is used in place of Y^0 in the inequality (13). Hence the octahedral shear stress τ_0 is calculated, assuming Hooke's Law, and relaxed during the time interval Δt by a stress corresponding to a shear strain obtained from dislocation theory. It is seen that it is only the stress corresponding to the plastic strain $\dot{\gamma}\,\Delta t$ that is removed by scaling the components of τ_0.*

The plastic shear strain can be obtained by:

$$\gamma = \int \dot{\gamma}\, dt \tag{15}$$

and is equal to the octahedral plastic shear, i.e., $\gamma = \gamma_0$.

$$\gamma_0 = 2/3 \sqrt{\left(P_{\epsilon_1} - P_{\epsilon_2}\right)^2 + \left(P_{\epsilon_2} - P_{\epsilon_3}\right)^2 + \left(P_{\epsilon_3} - P_{\epsilon_1}\right)^2} \tag{16}$$

where P_{ϵ_1}, P_{ϵ_2}, P_{ϵ_3} are the principal plastic strain components.

When the physical parameters in the expressions for the dislocation density and velocity are such that $\dot{\gamma}$ is very large then the yield strength, τ_y, will relax immediately to a static value $\tau_y = \tau_R$ [Eq. (14) with $\tau_{WH} = 0$]. Thus a material behaviour that corresponds to an elastic-perfectly plastic is obtained. A material behaviour where $\dot{\gamma}$ is large would be termed rate <u>independent</u> because the rate dependence could not be detected unless a very short time scale were used. The other extreme is when $\dot{\gamma}$ is always zero. This corresponds to a material that can sustain unlimited distortion and remain elastic. Actually to complete the model, the upper limit of crystal strength should be a boundary condition.

Thus, a strain-rate sensitive material is one where $\dot{\gamma}$ is finite but not so large that the effect cannot be detected.

---

*The scaling is actually applied to components of τ_0 in the coordinates of the equations of motion.

Applications of Dynamic Yield

Figure 18 shows a calculation of the time history of a stress wave in a target plate produced by a flying plate of the same material. The elastic precursor is seen to attenuate as the wave proceeds through the material. The geometry and physical constants were taken from Ref. 4. The rate of attenuation of the precursor is consistent with the experimental results of Ref. 4 and Ref. 6.

Figure 19 is a calculation of a flying aluminum plate striking an aluminum target plate. The initial dislocation density is $N^0 = 10^6$. Work hardening was introduced in the calculation such that the material strength increased a factor of three in addition to the static strength. The step behind the shock front is due to the elastic release wave. The step is less pronounced if work hardening is not introduced. These results are consistent with the experimental work of Ref. 7. The experiments by Bridgeman (1937) and Vereschagin (1960) indicate that the strength of materials increases with the pressure. However, recent work by R. E. Riecker[8] suggests that the increase in strength is in reality due to work hardening.

Figure 20 is a calculation of a mild steel cylinder striking a hard steel target. The dislocation parameters for the cylinders are the same as those used in Fig. 18. The final shape of the cylinder is almost identical to a similar problem done with elastic-plastic theory without dynamic yielding. Comparison of the cylinder shape where work hardening was included does show a difference, Fig. 20A.

In conclusion, it is not thought that the inclusion of dynamic yielding into the calculation program will significantly change the results from elastic-plastic theory for metals. However, it is expected that dynamic effects will be an important aspect of the fracture phenomenon in ceramic materials.

RESULTS OF EXPERIMENTS AND CALCULATIONS

Effects on the Target

The primary purpose of these experiments was to check out the computation program and the experimental measuring techniques. The calculational routines provided for a rupture failure to occur when the plastic distortion of a material zone exceeded 10%. The boundary conditions along a rupture were considered to be free surfaces or sliding interfaces. The calculations matched very well the experimental records of the projectile rear surfaces and the target front surfaces (see Fig. 10).

The calculations showed that the radius of the impact end of the cylinders increased as the cylinders penetrated the targets. At some point the edge could be expected to shear off and be left behind. Examination of the target showed that this

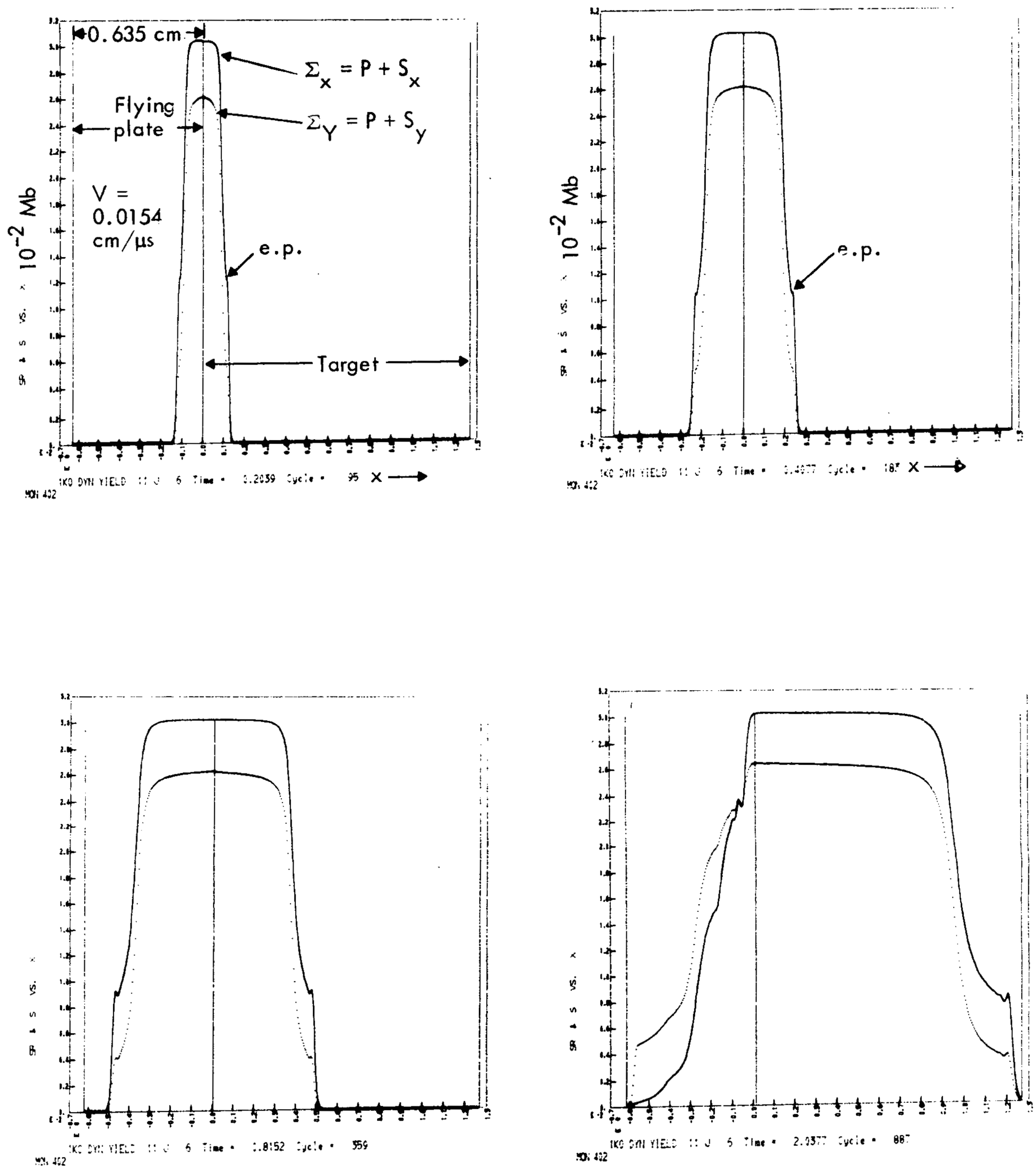

Fig. 18. Attenuation of an elastic precursor (e. p.) in Armco iron. Dynamic yield model.

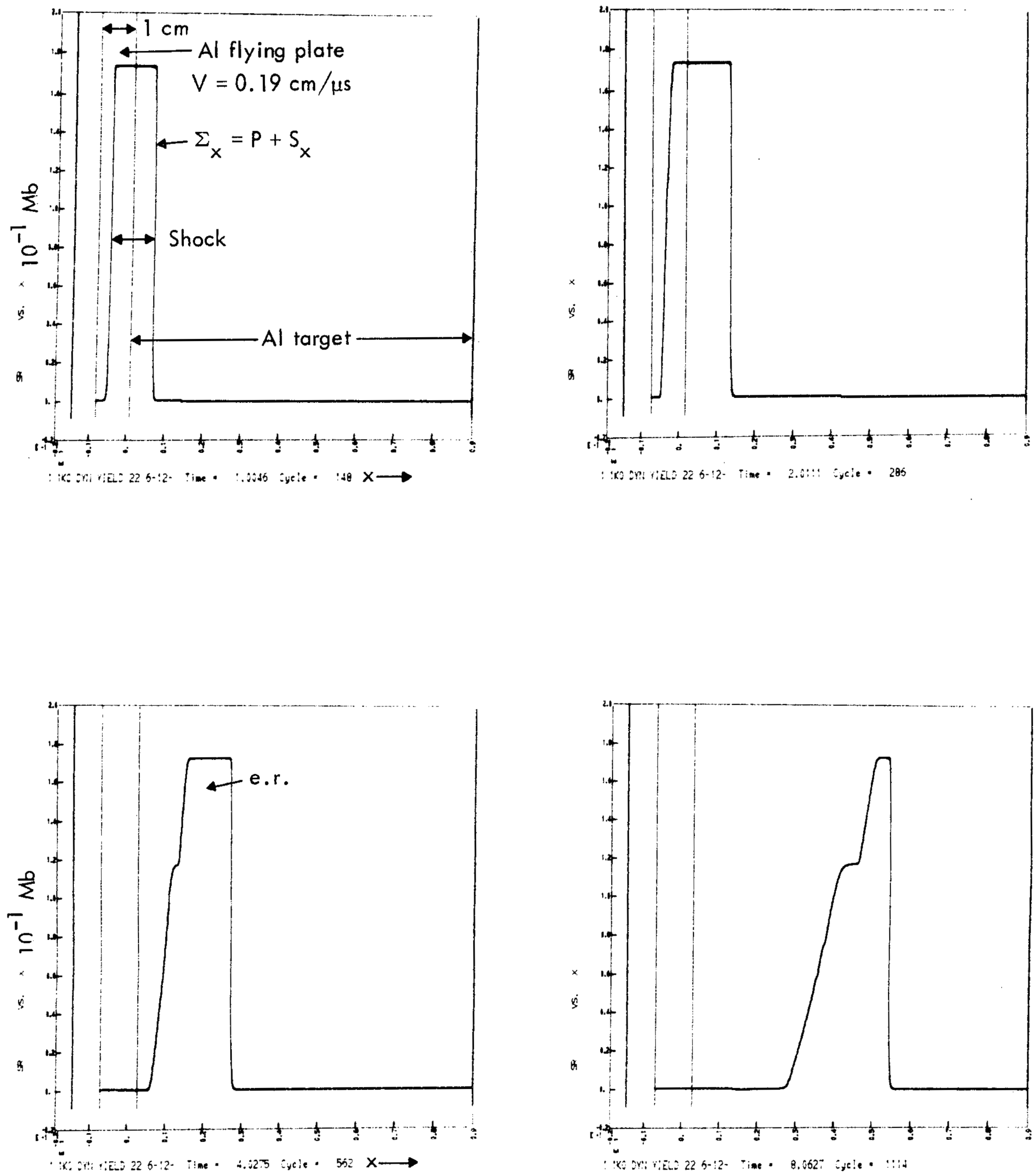

Fig. 19. Attenuation of a shock wave by an elastic rarefaction (e. r.) Dynamic yield model with work hardening.

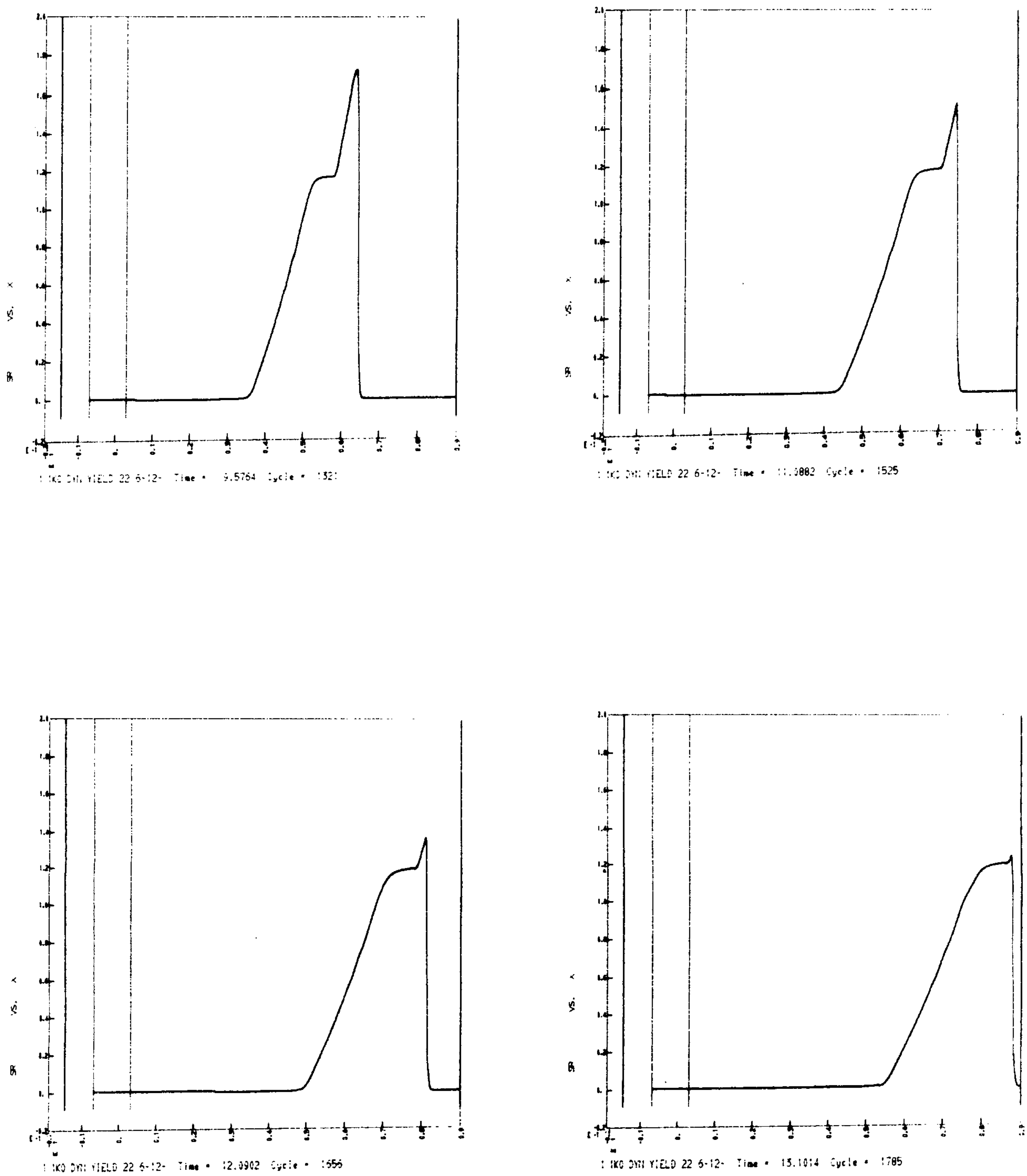

Fig. 19. Continued.

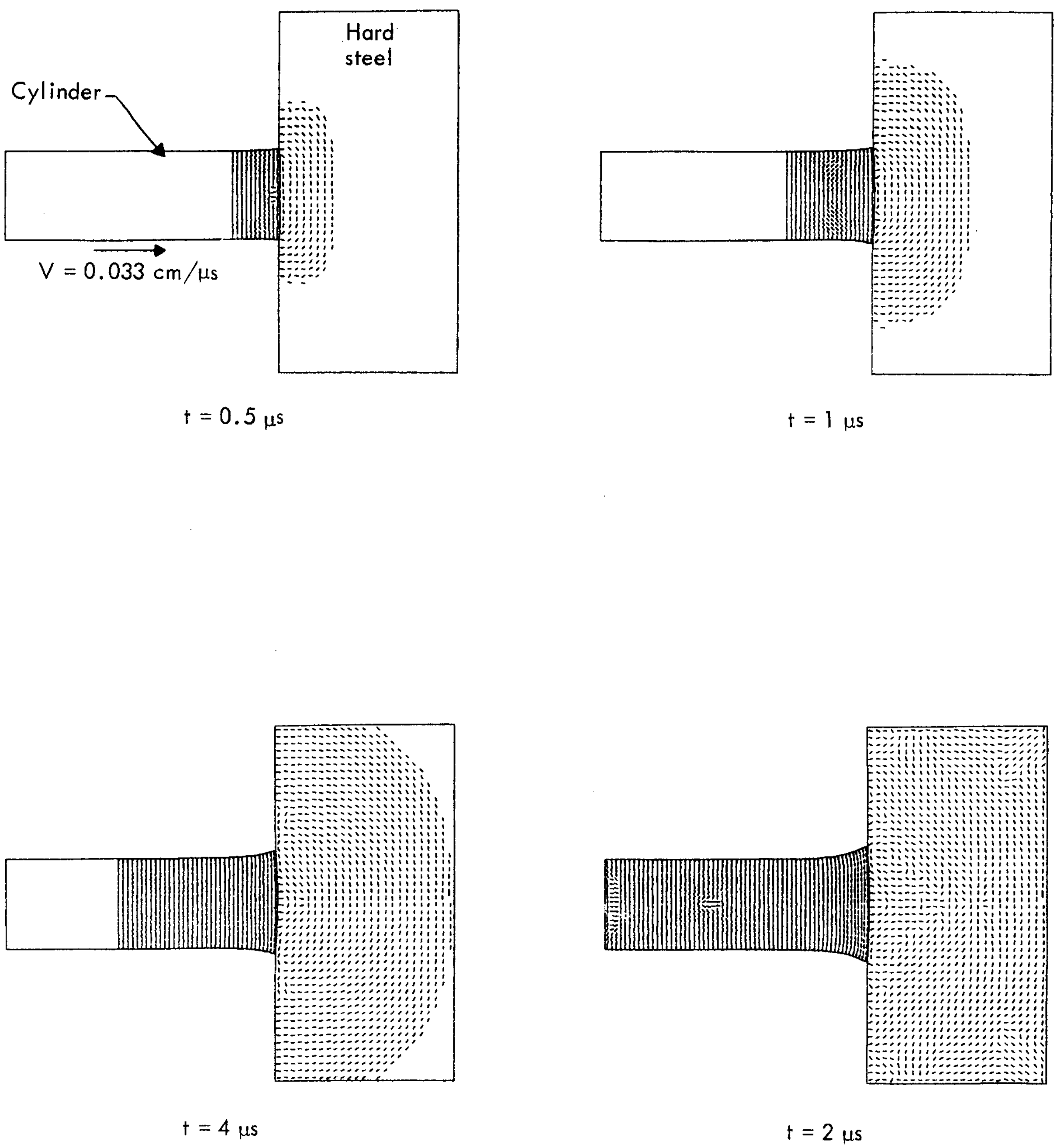

Fig. 20. Armco iron cylinder striking a hard steel plate. Dynamic yield model with work hardening for the cylinder material. The lines show the directions of the maximum principal stresses. (Lines of tension.)

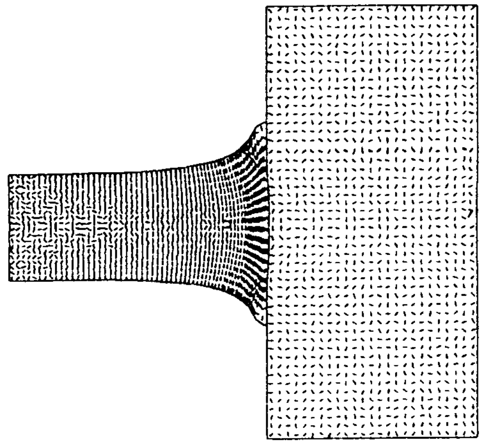

a) t = 25 μs

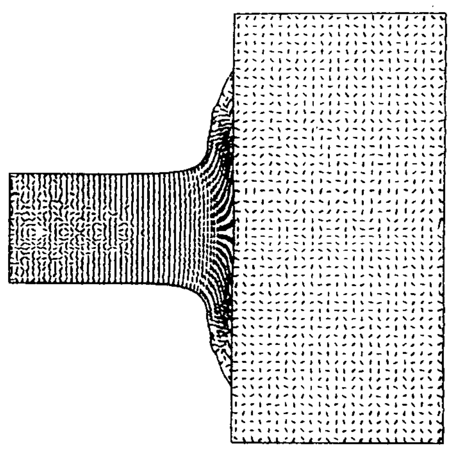

b) t = 25 μs

Fig. 20A. a) Continuation of Fig. 20.

b) Same initial conditions as (a) but elastic-plastic model for the cylinder material.

effect started to occur after penetration of about one cylinder radius. The change in the cylinder cross-sectional area helps decelerate the cylinders (see Figs. 21 and 22). Compression waves move back to the rear surface of the cylinder and change the slope (point 2, Fig. 10).

Figure 6 shows a cylinder that was stopped by a 1-1/2 in. aluminum target. About 1/3 of the cylinder has been stripped off. A rezone routine used with the computer calculations can take into account the loss of cylinder material as it penetrates the target. However, it is not thought that any new information would be obtained by calculating this experiment.

Streak camera records of the projectile rear surface and the target front surface were identical for the experiment shown in Figs. 8 and 9. These data and the other cylinder experiments are consistent with the assumption that the target fails in compression, i.e., the rarefactions in the target have little effect.

Figure 1 shows a pointed cylinder penetrating a 1 in. thick aluminum target. The corresponding calculation is shown in Fig. 23 (the projectile velocity used in the calculation was slightly less than the experimental value).

Effects on Projectiles

For a given areal density a greater projectile velocity is required to penetrate hard ceramic-faced armor than is required for single-component armor. Experiments with 30-calibre AP bullets show that V_{50} is proportional to the areal density to the 1.7 power for ceramic faced armor and to the 0.5 power for single-component armor. (V_{50} is the projectile velocity that defeats a given areal density for 50% of the experiments.) This change in the dependence of areal density on the velocity indicates that a different mechanism occurs during the penetration. Flash x ray offers the means to study what is happening in the projectile as it penetrates a target. Three heads of a 600-kV FXR system (Fig. 3) were set up to view targets of Al_2O_3 backed by aluminum. The FXR system can penetrate 2 in. of Al_2O_3 so the target materials were cut to this thickness. The projectiles struck the centers of the 2 in. strips. Figures 16 and 17 show the results of two experiments where the Al_2O_3 was backed by 1/2 in. aluminum and by 1/8 in. aluminum. The target with the 1/2 in. aluminum stopped the projectile whereas the system with 1/8 in. aluminum was completely penetrated. The projectiles in each experiment were pointed cylinders, type b, Fig. 1 with a velocity of 3050 ft/sec. It can be seen that the Al_2O_3 destroys the pointed shape of the projectiles, thus turning them into blunt cylinders. It is thought that with more data a model can be developed that relates the rate that the pointed cylinder is turned into a blunt cylinder with the depth of penetration. Once this is done it should be possible to derive the areal density dependence on the ballistic limit, V_{50}.

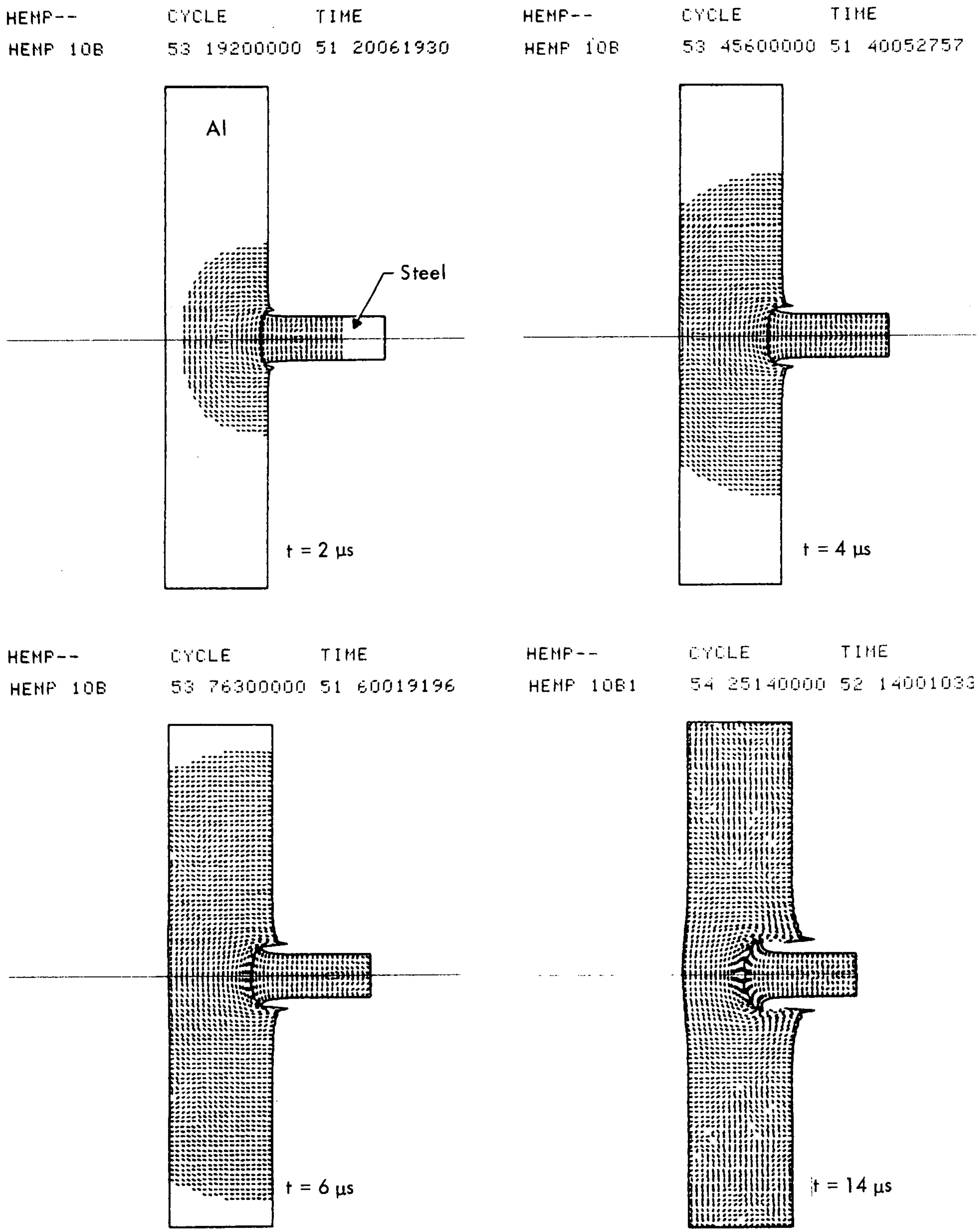

Fig. 21. Calculation of the penetration of a 3/4 in. thick aluminum plate by a steel cylinder (type C). Cylinder velocity, 0.091 cm/μsec. The lines indicate the direction of the maximum principal stress (lines of tension).

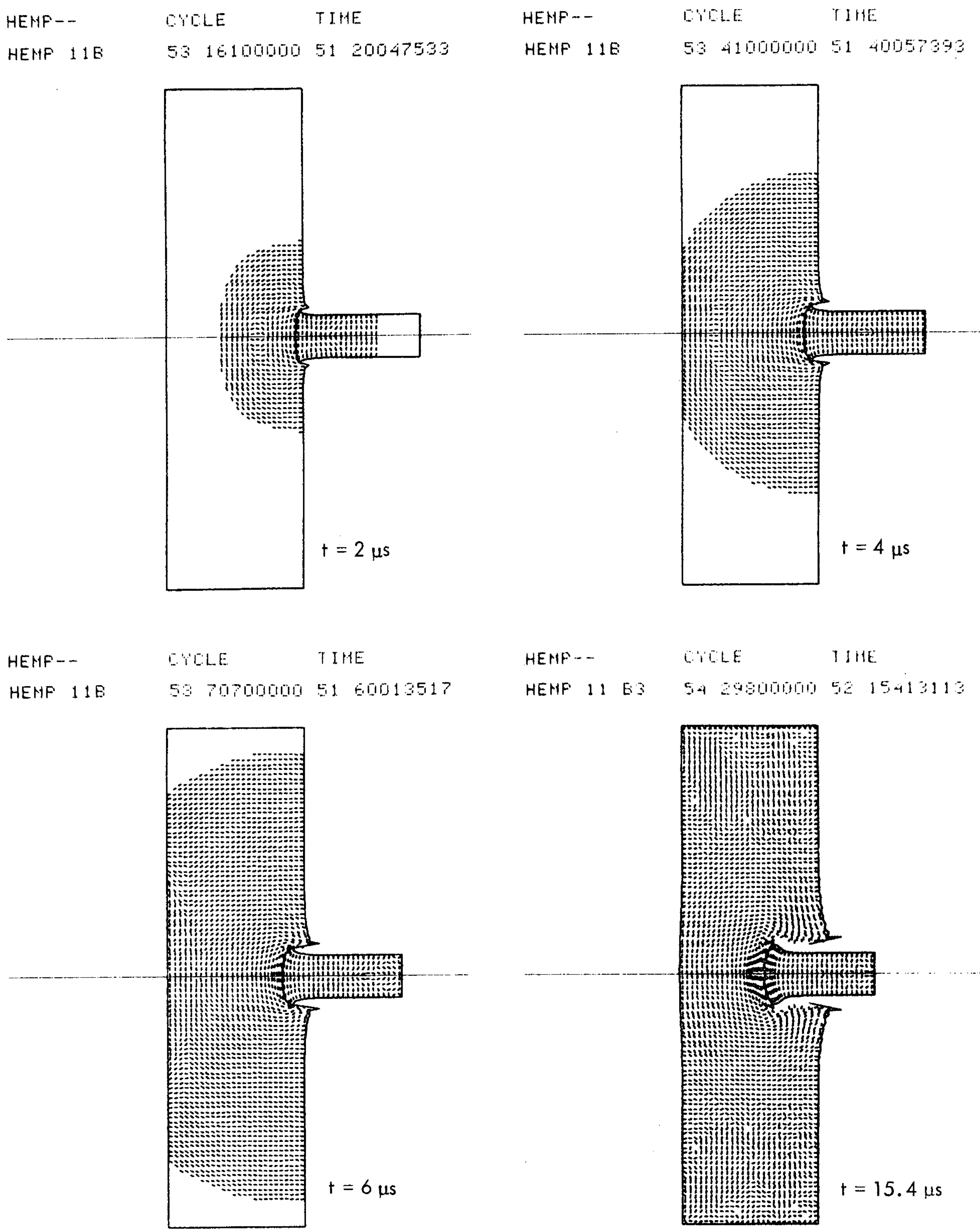

Fig. 22. Calculation of the penetration of a 1 in. thick aluminum plate by a steel cylinder (type C). Cylinder velocity 0.095 cm/μsec.

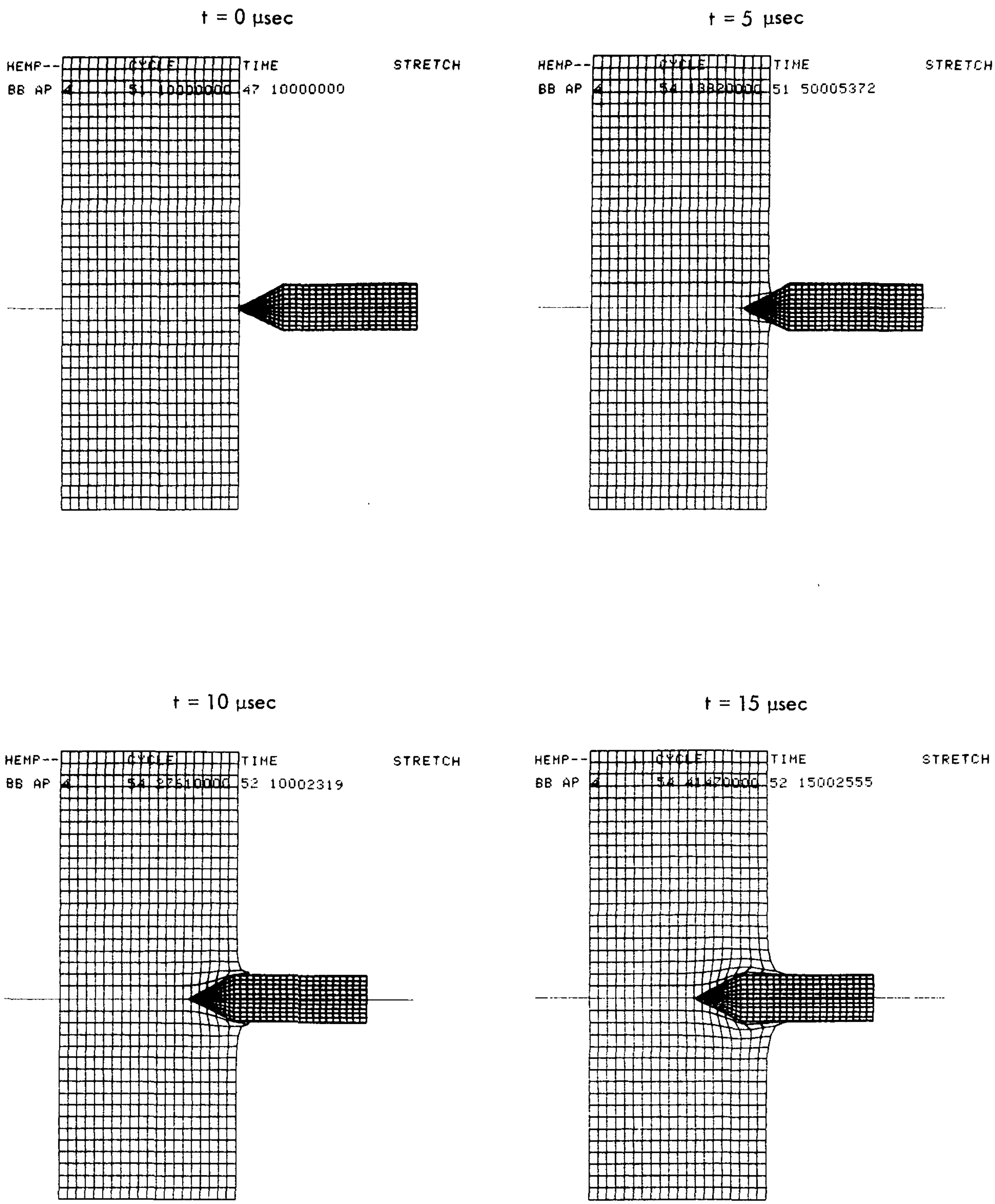

Fig. 23. Preliminary calculation of a steel projectile penetrating a 1 in. aluminum target. (No material strength was included in the aluminum.) Projectile velocity = 0.08 cm/μsec.

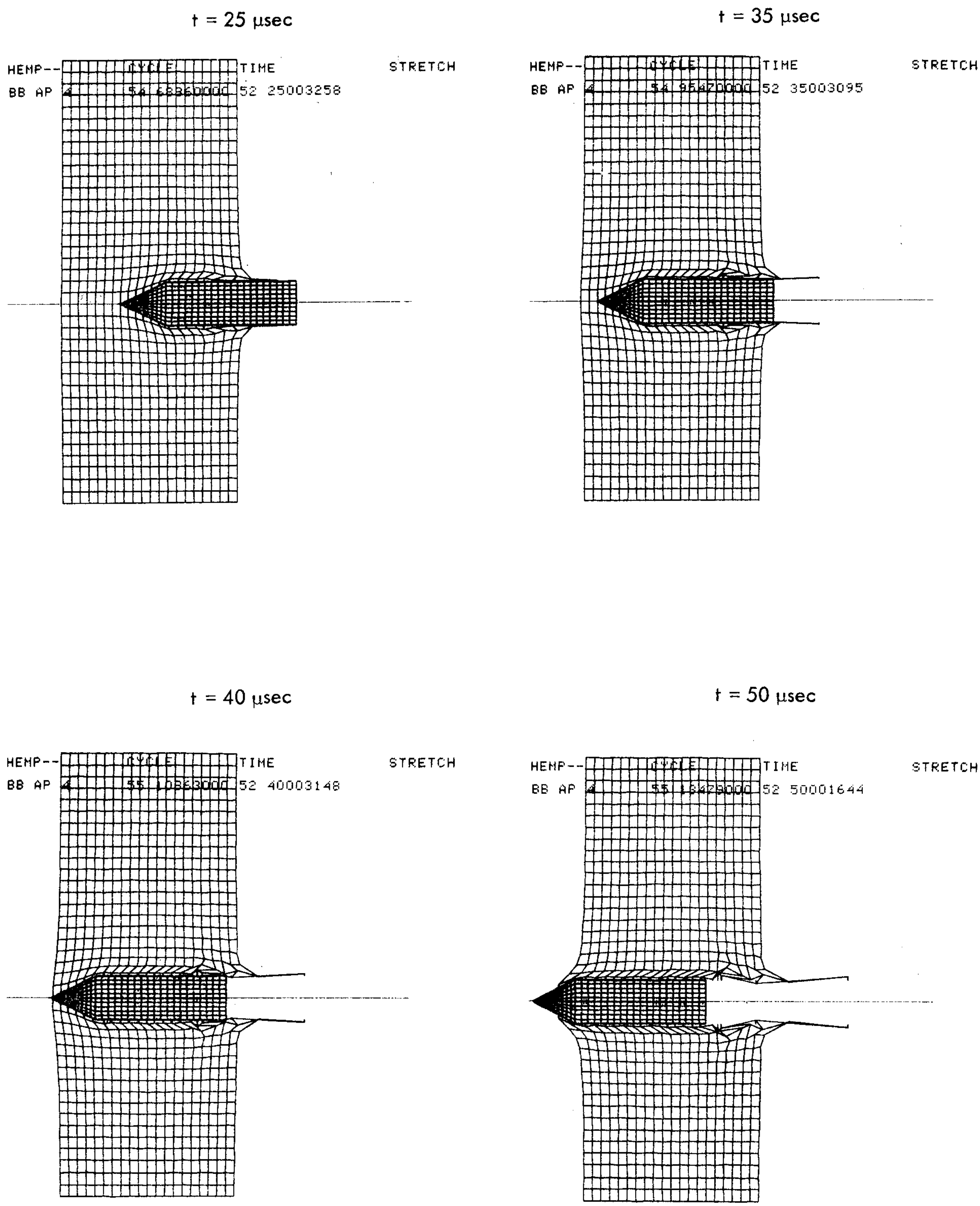

Fig. 23. (continued)

For example, a reasonable assumption is that the cross-sectional area A, of the pointed cylinder increases as the square of the distance, X, that the projectile penetrates in the ceramic.

$$A = KX^2.$$

Let

S_c = the ceramic compressive strength,
M = projectile mass,
V = projectile velocity.

Then

$$M\ V\ dV/dX = S_c\ A = S_c\ K\ X^2\ ,$$
$$M\ V\ dV = S_c\ K\ X^2\ dX\ ,$$
$$MV^2/2 = S_c\ K\ X^3/3\ ,$$

or

$$V_{50}^2 \propto S_c\ K/\rho^3\ (\rho X)^3\ , \qquad \text{where } \rho = \text{target density}$$

$$V_{50} \quad (SK/\rho^3)^{1/2}\ (\rho X)^{3/2}\ .$$

This analysis shows a 1.5 power V_{50} dependence on the areal density, (ρX), compared to the experimental 1.7.

ACKNOWLEDGMENTS

The authors wish to express their appreciation to Fred Johansen for his mechanical engineering support and to Robert C. Hansen for his electronic engineering support. Also to Dick Giroux and John French for writing the computer programs.

REFERENCES

[1] M. L. Wilkins, Methods in Computational Physics Vol. 3, Academic Press Inc., N. Y. (1964).

[2] W. G. Johnston and J. J. Gilman, J. Appl. Phys. 30, 129 (1959).

[3] J. J. Gilman, Australian J. Phys. 13, 327 (1960).

[4] J. W. Taylor, J. Appl. Phys. 36, 3146 (1965).

[5] J. N. Johnson, Shock Waves in Stress-Relaxing Solids, WSU SDL 66-01 (1966).

[6] J. W. Taylor and M. H. Rice, J. Appl. Phys. 34, 364 (1963).

[7] D. R. Curran, J. Appl. Phys. 34, 2677 (1963).

[8] R. E. Riecker, Air Force Cambridge Research Laboratories, private communication.

DISTRIBUTION

<u>LRL Internal Distribution</u>

Michael M. May	
M. Wilkins	100
TID File	30

<u>External Distribution</u>

Division of Technical Information Extension, Oak Ridge

JW/rt